TLR7 promotes smoke-induced lung damage through the activity of mast cell tryptase

Tatt Jhong Haw[1#], Malcolm R. Starkey[1,2#], Stelios Pavlidis[3], Sheena Tam[4], Prema M. Nair[1], Gang Liu[5], Henry M. Gomez[1], Irwan Hanish[1,6], Alan CY. Hsu[1], Richard Y. Kim[1,5], Ryutaro Fukui[7], Yusuke Murakami[8], Jay C. Horvat[1], Paul S. Foster[1], Brian GG. Oliver[9], Peter A. Wark[1], Ian M. Adcock[3], Kensuke Miyake[7], Don D. Sin[4] & Philip M. Hansbro[1,5*]

[1]Priority Research Centre for Healthy Lungs &/or Grow Up Well, Hunter Medical Research Institute & University of Newcastle, Callaghan, New South Wales, Australia. [2]Depatrment of Immunology and Pathology, Central Clinical School, Monash University, Melbourne, Victoria, Australia. [3]The Airways Disease Section, National Heart & Lung Institute, Imperial College London, London, UK. [4]The University of British Columbia Centre for Heart Lung Innovation, St Paul's Hospital & Respiratory Division, Dept of Medicine, University of British Columbia, Vancouver, BC, Canada. [5]Centre for Inflammation, Centenary Institute, and Faculty of Science, University of Technology Sydney, New South Wales, Australia. [6]Department of Microbiology, Faculty of Biotechnology and Biomolecular Sciences, Universiti Putra Malaysia, Serdang, Selangor, Malaysia. [7]Division of Innate Immunity, Department of Microbiology and Immunology, The Institute of Medical Science, The University of Tokyo, Shirokanedai, Minatoku, Tokyo, Japan. [8]Faculty of Pharmacy, Department of Pharmaceutical

Sciences, Musashino University, Nishitokyo-shi, Tokyo, Japan. [9]Woolcock Institute of Medical Research, University of Sydney & School of Life Sciences, University of Technology, Sydney, Australia.

[#]Authors contributed equally

*Correspondence and requests for reprints should be addressed to Philip M Hansbro, Ph.D., The Centre for Inflammation, Centenary Institute, and Faculty of Science, University of Technology Sydney, Australia. Phone: +61 2 9565 6248; Fax: +61 2 9565 6101; Email: philip.hansbro@uts.edu.au

Abstract word count: 100 (max 100)

Article word count: 3,898 (max 4,000)

Toll-like receptor (TLR)7 is known for eliciting immunity against single-stranded RNA viruses. TLR7 was increased in both human and cigarette smoke (CS)-induced experimental chronic obstructive pulmonary disease (COPD). Severity of CS-induced emphysema and COPD was reduced in TLR7-deficient mice whilst inhalation of imiquimod (TLR7-agonist) induced emphysema in naïve mice. Imiquimod-induced emphysema was reduced in mice treated with mast cell stabilizer cromolyn or deficient in mast cell protease-6. Therapeutic treatment with anti-TLR7 monoclonal antibody suppressed CS-induced emphysema, experimental COPD and accumulation of pulmonary mast cells. We demonstrate an unexpected role for TLR7 in mediating emphysema and COPD through mast cell activity.

Lung damage in respiratory disease is the most prolific cause of illness death globally. Chronic obstructive pulmonary disease (COPD) is the third leading cause of mortality worldwide and imposes an enormous socioeconomic burden[1]. It is complex and heterogeneous characterized by chronic pulmonary inflammation, airway remodeling, emphysema and progressively declining lung function[2]. A major risk factor is cigarette smoke (CS) inhalation whilst other exposures such as wood smoke and air pollution are also important[3]. Emphysema is associated with airway inflammation and progressive disease irrespective of smoking status[4]. Current therapies include smoking cessation, glucocorticoids, β2-adrenergic agonists and anticholinergic antagonists[5–7]. However, they only provide some symptomatic relief, and do not suppress causal factors, reverse the disease or halt its progression[7]. Hence, COPD lacks effective treatments, which is largely due to the poor understanding of underlying disease mechanisms.

Toll-like receptor (TLR)7 is an intracellular pattern recognition receptor (PRR) with well-known roles in host defense against single-stranded (ss)RNA viruses including influenza A and SARS-CoV-2 virus[8–12]. When ssRNA interacts with TLR7, myeloid differentiation primary response gene (MyD)88 is recruited. This leads to the activation of nuclear factor kappa-light-chain-enhancer of activated B cells (NF-κB) that drives inflammatory responses[8,9]. TLR7 may also signal through TIR-domain-containing adapter-inducing interferon (IFN)-β (TRIF) to activate IFN regulatory factors (IRFs), which drive the production of anti-viral type-I IFNs[8,9].

In the lung, TLR7 has pathogenetic roles in asthma[13–16]. TLR7 agonists suppressed levels of pro-inflammatory cytokines (interleukin [IL]-4, IL-5, IL-13) and airway inflammation, fibrosis and hyperresponsiveness in experimental asthma[13–16]. Mast cells are important inflammatory cells in asthma and COPD[17–21]. They express several PRRs, including TLR7[22–24], as well as cell-specific tetramer-forming tryptases (e.g. mouse MC protease-6

[mMCP-6], human (h)Tryptase-β)[25,26]. However, the role of TLR7 in COPD/emphysema is unknown, and there are no known links between TLR7 and mast cell-specific mediators.

We assessed the role of TLR7 in COPD pathogenesis using human data and CS-induced experimental COPD[25–37]. *Tlr7* mRNA levels were increased in both human and experimental COPD. TLR7-deficient (*Tlr7*$^{-/-}$) mice had reduced CS-induced emphysema-like alveolar enlargement that was associated with attenuated airway remodeling, apoptosis and mast cell numbers in the lungs and experimental COPD. The TLR7-agonist imiquimod increased CS-induced emphysema, apoptosis and mast cells in naive mice. Imiquimod-induced emphysema and apoptosis were ablated by the mast cell stabilizer cromolyn and in *mmcp6*$^{-/-}$ mice. CS-induced emphysema, apoptosis, airway remodeling and mast cells were reduced in mice following therapeutic neutralization of TLR7. Thus, we identify a previously unrecognized role for TLR7 in COPD pathogenesis and its potential as a novel therapeutic target.

RESULTS

TLR7 is increased in human and experimental COPD

We first assessed *TLR7* mRNA levels in pre-existing human microarray data from the Global Initiative for Chronic Obstructive Lung Disease (GOLD) stage I (mild), II (moderate) and IV (severe) COPD and non-COPD subjects[38–40]. *TLR7* mRNA was not different in airway epithelial brushings[40] from healthy smokers without COPD compared to non-smokers (**Fig. 1a**). However, it was increased in airway epithelial brushings from mild-to-moderate COPD patients compared to non-smokers and healthy smokers without COPD. *TLR7* mRNA was also increased in lung parenchyma[38,39] from severe COPD patients compared to subjects without COPD (**Fig. 1b**). Endogenous host RNA may induce TLR7 to drive disease[41,42]. Thus, we assessed the levels of anti-Smith antibody against endogenous RNA[43]. Levels inversely correlated with lung function impairment in 40 COPD patients (forced expiratory volume in 1

second [FEV_1] <80% of predicted, FEV_1 to FVC ratio <0.70 post-bronchodilator[44], **Fig. 1c, Supplementary Table 1**).

We next assessed *Tlr7* mRNA levels in the lungs in experimental COPD. Wild-type (WT) BALB/c mice were exposed to nose-only inhalation of CS or normal air and sacrificed after 4, 6, 8 and 12 weeks (**Fig. 1d**) as described previously[25–37]. *Tlr7* mRNA was increased after 6, 8 and 12 weeks of CS exposure (**Fig. 1e**), in both airways and lung parenchyma (**Fig. 1f** and **g**) compared to air-exposed controls. We also found increased TLR7 protein levels in small airway epithelial cells and parenchyma-associated inflammatory cells in CS-exposed mice (**Fig. 1h**).

CS-induced experimental COPD/emphysema is reduced in *Tlr7*$^{-/-}$ mice

We next determined that TLR7 has a role in CS-induced emphysema-like alveolar enlargement. WT and *Tlr7*$^{-/-}$ BALB/c mice were exposed to CS or normal air for 8 weeks[25–37]. CS-exposed WT mice had increased alveolar septal damage (**Fig. 1i**) and diameter (**Fig. 1j**) compared to air-exposed WT controls. In contrast, CS-exposed *Tlr7*$^{-/-}$ mice had no septal damage and only marginally increased alveolar enlargement compared to air-exposed *Tlr7*$^{-/-}$ and CS-exposed WT controls. These reductions in alveolar damage and diameter were associated with reduced terminal deoxynucleotidyl transferase dUTP nick end labeling $(TUNEL)^+$ cells in the parenchyma, indicating reduced apoptosis, in CS-exposed *Tlr7*$^{-/-}$ compared to CS-exposed WT controls (**Fig. 1k**).

We previously showed that mice develop small airway remodeling in experimental COPD[25,26,33]. CS exposure of WT and *Tlr7*$^{-/-}$ mice increased small airway epithelial cell area (thickening) compared to their respective air-exposed controls (**Fig. 1l**, **Supplementary Fig. 1a**). Notably, however, CS-exposed *Tlr7*$^{-/-}$ mice had reduced small airway epithelial cell thickening compared to CS-exposed WT controls.

We then determined whether reduced epithelial cell thickening was associated with decreased numbers of nuclei, an indicator of reduced numbers of epithelial cells. CS exposure of WT and *Tlr7*$^{-/-}$ mice increased nuclei numbers compared to their respective air-exposed controls (**Fig. 1m**, **Supplementary Fig. 1b**). However, CS-exposed *Tlr7*$^{-/-}$ mice had reduced small airway nuclei numbers compared to CS-exposed WT controls.

Next, we defined the effect of TLR7 on lung function in terms of transpulmonary resistance[33]. CS exposure of WT and *Tlr7*$^{-/-}$ mice increased transpulmonary resistance compared to air-exposed WT and *Tlr7*$^{-/-}$ controls (**Fig. 1n**). Transpulmonary resistance was not different between CS-exposed WT and *Tlr7*$^{-/-}$ mice. We also assessed the role of TLR7 in CS-induced pulmonary inflammation, mRNA levels of pro-inflammatory cytokines/chemokines and COPD-related factors in lung homogenates and interferon-related factors (**Supplementary Fig. 2a-y**). These were not different between CS-exposed WT and *Tlr7*$^{-/-}$ mice.

Administration of TLR7 agonist imiquimod induces experimental COPD/emphysema

We then assessed the effects of chronic intranasal (i.n) administration of imiquimod in the absence of CS for 8 weeks (**Fig. 2a**). Imiquimod administration to WT mice increased alveolar septal damage and diameter compared to saline-administered WT controls (**Fig. 2b** and **c**). These effects were associated with increased TUNEL^{+} parenchyma cells (**Fig. 2d**). Imiquimod also increased transpulmonary resistance (**Fig. 2e**).

Imiquimod administration to WT mice did not alter inflammatory cell numbers in bronchoalveolar lavage fluid (BALF), histopathology scores, small airway epithelial cell thickening or nuclei numbers, or interferon-related mRNA levels (**Supplementary Fig. 3a-p**).

Imiquimod administration increases severity of experimental COPD/emphysema

We next determined if exogenous imiquimod affects CS-induced experimental COPD. WT mice were exposed to CS or normal air for 8 weeks and administered sterile saline or imiquimod i.n between weeks 6-8 (**Fig. 2f**). Imiquimod administration to CS-exposed mice further increased alveolar septal damage (**Fig. 2g**) and diameter (**Fig. 2h**) compared to imiquimod-administered air-exposed and, saline-administered CS-exposed controls. Notably, imiquimod-administered air-exposed mice also had increased alveolar septal damage and diameter compared to saline-administered air-exposed controls. Increased alveolar septal damage and diameter in imiquimod-administered CS- and air-exposed mice were associated with increased $TUNEL^{+}$ parenchyma cells (**Fig. 2i**). Then, we assessed the effects of imiquimod on lung function. Saline-administered CS-exposed mice had increased transpulmonary resistance compared to saline-administered air-exposed controls (**Fig. 2j**). In contrast, resistance was not altered in imiquimod-administered CS-exposed mice compared to imiquimod-administered air-exposed controls. This was because increased resistance occurred in imiquimod-administered compared to saline-administered air-exposed controls. Imiquimod-administered CS-exposed mice had increased resistance compared to saline-administered CS-exposed controls.

Imiquimod did not alter the numbers of inflammatory cells in BALF, histopathology score, small airway epithelial cell thickening or nuclei numbers and had minimal effects on interferon-related mRNA levels (**Supplementary Fig. 4a–p**).

Imiquimod-induced emphysema is TLR7- and MyD88-dependent

Next, we determined if imiquimod-induced emphysema is a short-term effect and is TLR7- and MyD88-dependent. We administered saline or imiquimod acutely i.n to WT, *Tlr7*$^{-/-}$ or *Myd88*$^{-/-}$ mice for 2 weeks (**Fig. 3a**). Short-term imiquimod increased alveolar septal damage (**Fig. 3b**) and diameter (**Fig. 3c**) in WT mice compared to saline-administered controls. These

effects were significantly reduced in imiquimod-administered *Tlr7*$^{-/-}$ compared to WT controls. This was associated with reduced TUNEL^{+} parenchyma cells (**Fig. 3d**) and reduced transpulmonary resistance (**Fig. 3e**).

Notably, imiquimod-induced alveolar septal damage (**Fig. 3f**) and diameter (**Fig. 3g**) were similarly significantly reduced in *Myd88*$^{-/-}$ compared to imiquimod-administered WT controls. These were also associated with reduced TUNEL^{+} parenchyma cells (**Fig. 3h**) and transpulmonary resistance (**Fig. 3i**).

Acute imiquimod administration did not alter the numbers of inflammatory cells in BALF, histopathology scores, small airway epithelial cell thickening or nuclei numbers or interferon-related mRNA levels in *Tlr7*$^{-/-}$ (**Supplementary Fig. 5a-o**) or *Myd88*$^{-/-}$ mice (**Supplementary Fig. 6a-o**).

Imiquimod promotes pulmonary mast cell influx

We and others showed that mast cells are involved in human and experimental COPD[19–21,25,26]. Given that certain population of mast cells express TLR7[22–24], we next assessed the numbers of pulmonary mast cells in mice administered imiquimod for 8 weeks (**Fig. 2a**) or during weeks 6-8 of CS exposure (**Fig. 2f**). Chronic imiquimod administration increased pulmonary mast cell numbers compared to saline-administered controls (**Fig. 4a**). Imiquimod-induced pulmonary mast cell influx was TLR7- (**Fig. 4b)** and MyD88-dependent (**Fig. 4c)**. Consistent with our previous studies[25,26], pulmonary mast cell numbers were increased in saline-administered CS-exposed compared to air-exposed controls (**Fig. 4d**). Imiquimod increased pulmonary mast cells in CS- and air-exposed mice compared to respective saline-administered CS- and air-exposed controls.

Imiquimod-induced emphysema is ablated by cromolyn administration and in *mmcp6*$^{-/-}$ mice

Next, we assessed the impact of cromolyn on imiquimod-induced emphysema. Cromolyn stabilizes and prevents mast cell degranulation and the release of their contents including tryptases[45]. WT mice were administered cromolyn followed by imiquimod 2 hours later i.n for 2 weeks (**Fig. 4e**). Cromolyn had no effect on saline-administered control mice. Imiquimod administration increased alveolar septal damage (**Fig. 4f**) and diameter (**Fig. 4g**), TUNEL^{+} parenchyma cells (**Fig. 4h**, **Supplementary Fig. 7**) and transpulmonary resistance (**Fig. 4i**) compared to vehicle-administered controls. Each of these imiquimod-induced effects were ablated in cromolyn-treated mice compared to vehicle-administered controls. Cromolyn or imiquimod did not alter inflammatory cell numbers in BALF, histopathology scores, small airway epithelial cell thickening or nuclei numbers (**Supplementary Fig. 8a-k**).

We previously demonstrated that the mast cell-specific tryptases, mMCP6 and protease serine member S (Prss)31, play critical roles in experimental CS-induced emphysema[25,26]. To assess the relationship between TLR7 and mast cell granule-specific tryptase, WT or *mmcp6*$^{-/-}$ C57BL/6 mice were administered imiquimod i.n for 2 weeks (**Fig. 4j**). Imiquimod administration to WT mice increased alveolar septal damage (**Fig. 4k**) and diameter (**Fig. 4l**) compared to saline-administered WT controls. In contrast, administration to *mmcp6*$^{-/-}$ mice did not increase alveolar septal damage or diameter compared to saline-administered *mmcp6*$^{-/-}$ controls. Increased alveolar septal damage and diameter were also inhibited compared to imiquimod-administered WT controls. These effects were associated with reduced TUNEL^{+} parenchyma cells in imiquimod-administered *mmcp6*$^{-/-}$ mice compared to imiquimod-administered WT controls (**Fig. 4m**, **Supplementary Fig. 9**). Imiquimod administration to WT or *mmcp6*$^{-/-}$ mice also increased transpulmonary resistance compared to their respective saline-administered controls (**Fig. 4n**). However, resistance was not different between imiquimod-

administered WT and *mmcp6*$^{-/-}$ mice. Imiquimod administration to WT or *mmcp6*$^{-/-}$ mice did not alter BALF inflammatory cell numbers, histopathology score, airway epithelial cell thickening or nuclei numbers (**Supplementary Fig. 10a–k**). To test if imiquimod-induced emphysema was dependent on secreted mast cell tryptase, we administered imiquimod to *Prss31*$^{-/-}$ mice that lack mast cell surface tryptase. Imiquimod induced emphysema was similar in *Prss31*$^{-/-}$ mice and WT controls (**Supplementary Fig. 11a** and **b**).

Imiquimod induces the release of mast cell tryptase from human mast cells

We next determined whether imiquimod induced tryptase release from human mast cells. First, we confirmed that human mast cell line 1 (HMC-1) cells expressed TLR7 by immunostaining (**Fig. 5a**). We then incubated HMC-1 cells with media or imiquimod (5, 10 or 100 ng) for 1 hour. HMC-1 cells incubated with media clearly expressed mast cell tryptase (**Fig. 5b**). The intensity of mast cell tryptase immunostaining reduced in HMC-1 cells incubated with increasing concentrations of imiquimod. This was confirmed when mast cell tryptase was quantified in terms of DAB signal (pixels) normalized to cell numbers (**Fig. 5c**) or area of hematoxylin-stained cells (**Fig. 5d**). Furthermore, mast cell tryptase activity dose-dependently increased in culture supernatants of HMC-1 cells incubated with imiquimod compared to media (**Fig. 5e**). Interestingly, other proteases such as neutrophil elastase, myeloperoxidase and total matrix metalloproteinase activities were not increased in the lungs of mice chronically administered imiquimod (**Supplementary Fig. 12a-c**).

Prophylactic TLR7 neutralization prevents CS-induced experimental COPD/emphysema

We previously showed that emphysema-like alveolar enlargement develops between weeks 6-8 of CS exposure in mice[25]. To assess the therapeutic potential of targeting TLR7, WT mice were exposed to CS or normal air for 8 weeks and treated with neutralizing anti-TLR7

monoclonal antibody or isotype control intravenously (i.v) between weeks 6-8 (**Fig. 6a**). Anti-TLR7-treated CS-exposed mice had increased alveolar septal damage (**Fig. 6b**) and diameter (**Fig. 6c** and **Supplementary Fig. 13a**) compared to air-exposed controls. However, importantly, alveolar damage and diameter were significantly reduced compared to isotype-treated CS-exposed controls. The reductions in CS-induced alveolar septal damage and diameter in anti-TLR7-treated mice were associated with reduced numbers of $TUNEL^{+}$ parenchyma cells, which were reduced to the baseline levels in isotype- or anti-TLR7 treated air-exposed controls (**Fig. 6d**, **Supplementary Fig. 13b**).

Small airway epithelial thickening (**Fig. 6e**, **Supplementary Fig. 13c**) and nuclei numbers (**Fig. 6f**, **Supplementary Fig. 13d**) were increased in CS-exposed mice administered either isotype or anti-TLR7 antibodies compared to their air-exposed controls. Notably, anti-TLR7 treatment reduced small airway epithelial cell thickening in CS-exposed compared to isotype-treated controls. Isotype- and anti-TLR7-treated CS-exposed mice had increased transpulmonary resistance compared to isotype- and anti-TLR7-treated air-exposed controls, respectively (**Fig. 6g**). Resistance was similar in anti-TLR7-treated and isotype-treated CS-exposed mice.

Isotype-treated CS-exposed mice also had increased mast cell numbers compared to isotype-treated air-exposed controls (**Fig. 6h**). Notably, anti-TLR7 treatment of CS-exposed mice prevented the increase in lung mast cell numbers compared to isotype-treated CS-exposed controls. Numbers were reduced to baseline levels in anti-TLR7-treated air-exposed controls. Consistent with this, CS-exposed *Tlr7*$^{-/-}$ mice did not have increased lung mast cell numbers compared to air-exposed *Tlr7*$^{-/-}$ controls, which were also reduced to baseline in air-exposed WT controls (**Fig. 6i**).

Notably, anti-TLR7-treatment reduced CS-induced BALF total leukocytes compared to isotype-treated controls (**Supplementary Fig. 14a**). This was due to the suppression of

macrophage but not neutrophil or lymphocyte numbers (**Supplementary Fig. 14b-d**). Anti-TLR7 treatment did not alter histopathology score in CS-exposed compared to isotype-treated controls (**Supplementary Fig. 14e-i**). Treatment partially restored IFN-α (*Ifna*) mRNA expression in CS-exposed mice (**Supplementary Fig. 14j**) but had no effect on IFN-β (*Ifnb*), -γ (*Ifng*), -λ (*Ifnl*) or IFN receptor-1 (*Ifnar1*) mRNA levels (**Supplementary Fig. 14k-n**).

Therapeutic anti-TLR7 treatment suppresses CS-induced experimental COPD/emphysema

We then assessed therapeutic treatment with anti-TLR7 monoclonal antibody to reduce experimental COPD progression and severity. WT mice were exposed to CS for 8 weeks until disease developed. Controls were exposed to normal air. Some mice continued to be CS-exposed and were treated with a neutralizing anti-TLR7 monoclonal antibody or isotype control intravenously (i.v) between weeks 8-12 to assess the effects of treatment on disease progression (**Fig. 6j**). Some mice underwent CS cessation after 8 weeks of CS exposure prior to assessing the effects of treatment from weeks 8-12 in reversing disease. Isotype and anti-TLR7 treatments had no effect on air-exposed mice. Isotype-treated continually CS-exposed and CS cessation mice had increased alveolar septal damage (**Fig. 6k**) and diameter (**Fig. 6l**, **Supplementary Fig. 15a**) compared to isotype-treated air-exposed controls. Anti-TLR7-treated continually CS-exposed groups had a slight increase in alveolar septal damage and diameter compared to anti-TLR7-treated air-exposed controls. Anti-TLR7-treated CS cessation groups were completely protected from alveolar septal damage and increased diameter, which were no different to levels in anti-TLR7-treated air-exposed controls. Most importantly, in both groups of anti-TLR7 treated CS-exposed mice alveolar septal damage and diameter were significantly and substantially reduced compared to isotype-treated continually CS-exposed

292 and CS cessation controls. This was associated with reduced numbers of $TUNEL^+$ parenchyma
293 cells (**Fig. 6m**).

294 Next, we assessed the impact of therapeutic anti-TLR7 treatment on small airway
295 remodelling. Small airway epithelial thickening (**Fig. 6n**, **Supplementary Fig. 15b**) and nuclei
296 numbers (**Fig. 6o**) were increased in continually CS-exposed and CS cessation mice treated
297 with either isotype or anti-TLR7 compared to their air-exposed controls. Notably, anti-TLR7
298 treatment reduced small airway epithelial cell thickening and nuclei number in CS-exposed
299 compared to isotype-treated controls.

300 We recently established the assessment of pulmonary gaseous exchange in mice in
301 terms of diffusing lung capacity for carbon monoxide (DL_{CO}) similar to that assessed in COPD
302 patients[28]. Isotype-treated continually CS-exposed and CS cessation mice had reduced gas
303 exchange compared to isotype-treated air-exposed controls (**Fig. 6p**). Anti-TLR7 treatment
304 completely restored gas exchange in the lungs of continually CS-exposed and CS cessation
305 mice back to baseline levels in air-exposed mice.

306 Isotype-treated continually CS-exposed and CS cessation groups also had increased
307 mast cell numbers compared to isotype-treated controls (**Fig. 6q**). Anti-TLR7 treatment
308 completely inhibited the increases in mast cell numbers back to anti-TLR7-treated air-exposed
309 control levels and were substantially reduced compared to isotype-treated CS-exposed
310 controls. The levels of BALF inflammatory cells were reduced in anti-TLR7 treated continually
311 CS-exposed mice compared to treatment with isotype control (**Supplementary Fig. 16a-d**).
312 Treatment did not alter histopathology scores in CS-exposed compared to isotype-treated
313 controls (**Supplementary Fig. 16e-i**).

314

315 **DISCUSSION**

316 This is one of the first demonstrations of non-viral related functions of TLR7, and the first to
317 show pathogenic roles and potential for therapeutic targeting in lung damage. We show that
318 TLR7 is increased in human and experimental COPD, and promotes alveolar destruction,
319 emphysema and experimental COPD through mast cell tryptase activity. This is unexpected
320 because of the known roles of TLR7 are in antiviral immunity and protection against infection-
321 induced exacerbations in respiratory diseases[8–10]. *Tlr7*$^{-/-}$ mice had reduced CS-induced
322 emphysema and airway remodeling and improved lung function and therefore experimental
323 COPD. These were associated with reduced apoptosis in the lungs. Conversely, imiquimod
324 stimulation of TLR7 induced emphysema and apoptosis in mouse lungs, which synergistically
325 increased with CS-exposure. Others showed that CS-exposed *Unc93b1* mutant (*Tlr3/7/9*$^{-/-}$)
326 mice also had significant reductions in alveolar enlargement[41], however, the specific
327 involvement of TLR7 was not elucidated. Imiquimod is pro-apoptotic against certain cancer
328 cells[46–49], and induces apoptosis in human and mouse cell lines[50]. Thus, our study is the first to
329 demonstrate unexpected and novel roles for TLR7 in apoptosis in the lung, emphysema and
330 experimental COPD.

331 Somewhat surprisingly, CS-induced pulmonary inflammation in BALF and tissues and
332 histopathology scores were not altered in *Tlr7*$^{-/-}$ mice. This is in contrast to *Unc93b1* mutant
333 mice that had reduced total leukocytes in BALF when exposed to CS for six months[41].
334 However, the observed reduction in BALF total leukocytes in that study was minor (~1.3-
335 fold)[41], and the effects may be consequential of global dysfunction of intracellular TLR
336 signaling. We found that CS-induced inflammatory mediators, chemokines and COPD-related
337 factors[25,30,33] were induced by CS exposure but were not altered in *Tlr7*$^{-/-}$ mice. This was
338 consistent with the inflammatory profile in *Tlr7*$^{-/-}$ mice. We also showed that TLR7 stimulation
339 with imiquimod or anti-TLR7 treatment did not alter CS-induced pulmonary inflammation.
340 Hence, TLR7 does not have a major role in CS-induced inflammation, and the effects on

emphysema and COPD are inflammation-independent. Instead, the effects are likely on the airway epithelium and we show small-airway remodeling changes and apoptosis may be linked to and promote emphysema[51].

Low dose imiquimod (50 μg) was used to mimic responses induced by CS exposure rather than viral infection. Acute viral infections induce excessive inflammatory cell infiltrates, cytokine and chemokine responses and virus-induced tissue destruction[52–54]. Inflammatory responses induced by CS exposure are chronic and low grade, and CS suppresses anti-viral IFN responses in certain immune cells[30,55,56]. We and others previously showed that CS exposure suppressed IFN responses, which increased susceptibility to lung infections that typify COPD exacerbations[30,57–61]. Intranasal administration of higher doses (100 μg) of another TLR7 agonist, gardiquimod, also did not induce significant type I IFN responses in the lung[62]. Some mice were also intranasally administered a similar dose of imiquimod (50 μg), but the effects on lung type-I IFN responses were not assessed[62].

In contrast, other studies demonstrated imiquimod-induced IFNs expression in other tissues[63–65]. Topical application of Aldara (62.5 mg, 5% imiquimod) induced psoriasiform skin inflammation and increased serum levels of IFN-α and -β in mice[63]. *Ifna2* mRNA levels were also induced in healthy human peripheral blood monocytes stimulated with imiquimod (10 μg/mL) *in vitro*[64]. Moreover, oral imiquimod administration (30 mg/kg) induced type-I *Ifn* mRNA levels in the gastrointestinal mucosa of mice[65]. The differences between our study and those of others may be in part due to differences in regimen, doses, route of administration and cell-/tissue-specific effects. In our experimental studies we showed that IFN responses were not altered in *Tlr7*$^{-/-}$ mice or with antibody neutralization of TLR7. Thus, targeting TLR7 in COPD may not predispose patients to increased risk of infectious exacerbations.

Mast cells express TLR7 and stimulation with the TLR7 agonist resiquimod induced their production of inflammatory cytokines and chemokines *in vitro*[22–24]. We previously

showed that mice deficient in mast cell-specific tryptases mMCP-6 and Prss31 were protected against CS-induced emphysema and experimental COPD[25,26]. However, it was not known whether TLR7 activation on mast cells leads to the release of tryptases that promote disease. We therefore assessed the impact of imiquimod administration on *mmcp6*$^{-/-}$ or *Prss31*$^{-/-}$ mice. Imiquimod-induced emphysema was significantly ablated in *mmcp6*$^{-/-}$, but not *Prss31*$^{-/-}$ mice. mMCP-6 is a soluble while Prss31 is a membrane-bound tryptase. This suggests that the effects of TLR7-induced emphysema are likely to involve soluble tryptases or mediators released from mast cells. Furthermore, we showed that the human mast cell line HMC-1 expressed TLR7 and stimulation with imiquimod increased mast cell tryptase activity in culture supernatants. Collectively, our study is the first to demonstrate a novel role of TLR7 in mast cells and provides new insights into the mechanisms of TLR7-driven emphysema and COPD.

TLR7 may detect and induce inflammatory responses to host-derived RNA released by apoptotic cells[24,41,42]. Thus, the levels of circulating RNA were determined indirectly by detecting the presence of anti-Smith antibody (a host RNA-specific auto-antibody)[43]. Serum anti-Smith antibody levels inversely correlated with impaired lung function in COPD patients. This suggests that the level of endogenous RNA may be increased in COPD. Supporting this, others showed experimentally that mice exposed to CS for six months had increased levels of nucleic acids (RNA, DNA) in BALF[41]. The release of nucleic acid was a consequence of apoptosis of the mouse lung epithelial cell line (MLE-15) exposed to CS extract *in vitro*[41]. Additionally, others showed that ssRNA stimulated TNF-α production in mouse macrophage (RAW-ELAM) and activated human macrophage-like (THP-1) cells in a TLR7-dependent manner[42]. Further investigation with a combination of TLR7 pulldown assays and mass spectrometry may be useful to determine whether CS interacts with TLR7. The impact of microbiomes and their component nucleic acids would also be interesting[66,67].

In summary, we discover an unexpected role for TLR7 in mediating emphysema and COPD through mast cell-specific tryptase activity (**Fig. 6r**). CS- and imiquimod-induced emphysema was TLR7- and MyD88-dependent but independent of inflammation and IFN responses. Our study provides new insights and possible mechanisms of how TLR7 potentiates tissue-specific responses through mast cells. Crucially, we also showed that prophylactic and therapeutic targeting of TLR7 reduced emphysema and experimental COPD, and concomitantly, lung mast cell numbers. Thus, our study identifies TLR7 as a promising treatment target and opens a new avenue for developing new therapeutic strategies to reduce or reverse the severity of emphysema and COPD, as well as mast cell-related diseases.

METHODS

Methods and any associated references are available in the online version of the paper.

Accession codes. Microarray data for TLR7 expression in human COPD are available under accession code GSE5058 and GSE27597.

Note: Any Supplementary Information and Source of Data files are available in the online version of the paper.

ACKNOWLEDGEMENTS

We thank Bradley Mitchell, Breanna Anderson, Kristy Wheeldon and Natalie Kiaos for assistance with CS exposure models. This work was funded by National Health and Medical Research Council (NHMRC) of Australia grants to P.M.H., B.G.G.O, P.A.W., I.M.A. and K.M. (1137995, 1023131). M.R.S. was supported by an Australian Research Council fellowship DE170100226. R.Y.K was supported by a fellowship from the Lung Foundation

Australia/Boehringer Ingelheim (2017/1). P.M.H. was supported by a fellowship and investigator grant from the NHMRC (1079187, 1175134).

AUTHOR CONTRIBUTIONS

T.J.H. and M.R.S. co-designed the study, performed the experiments, collected and analyzed the data, generated the figures and wrote the manuscript. S.P. analyzed microarray and generated the human data. S.T. and D.D.S. obtained, analyzed and generated human anti-Smith antibody data. P.M.N., G.L., H.M.G., I.H., A.C.H. and R.Y.K. assisted in performing and collecting lung function data from experiments. J.C.H., P.A.W., and P.S.F. provided advice on experimental design/analysis and edited the manuscript. R.F., Y.M. and K.M. produced and generously provided the neutralizing anti-TLR7 monoclonal antibody. D.D.S. and I.M.A. analyzed human data and edited the manuscript. P.M.H. conceived the ideas, designed the study, funded the study, oversaw the research program and edited the manuscript.

COMPETING FINANCIAL INTERESTS

The authors declare no competing financial interests.

REFERENCES

1. Lozano, R. *et al.* Global and regional mortality from 235 causes of death for 20 age groups in 1990 and 2010: a systematic analysis for the Global Burden of Disease Study 2010. *Lancet* **380**, 2095–2128 (2012).
2. Han, M. K. *et al.* Chronic obstructive pulmonary disease phenotypes: the future of COPD. *Am. J. Respir. Crit. Care Med.* **182**, 598–604 (2010).
3. Keely, S., Talley, N. J. & Hansbro, P. M. Pulmonary-intestinal cross-talk in mucosal inflammatory disease. *Mucosal Immunol.* **5**, 7–18 (2012).

4. Miller, M. *et al.* Persistent airway inflammation and emphysema progression on CT scan in ex-smokers observed for 4 years. *Chest* **139**, 1380–1387 (2011).
5. Willemse, B. W. M., Postma, D. S., Timens, W. & ten Hacken, N. H. T. The impact of smoking cessation on respiratory symptoms, lung function, airway hyperresponsiveness and inflammation. *Eur. Respir. J.* **23**, 464–476 (2004).
6. Spina, D. Pharmacology of novel treatments for COPD: are fixed dose combination LABA/LAMA synergistic? *Eur. Clin. Respir. J.* **2**, (2015).
7. Barnes, P. J. Corticosteroid resistance in patients with asthma and chronic obstructive pulmonary disease. *J. Allergy Clin. Immunol.* **131**, 636–645 (2013).
8. Kawai, T. & Akira, S. The role of pattern-recognition receptors in innate immunity: update on Toll-like receptors. *Nat. Immunol.* **11**, 373–384 (2010).
9. Crozat, K. & Beutler, B. TLR7: A new sensor of viral infection. *Proc. Natl. Acad. Sci.* **101**, 6835–6836 (2004).
10. To, E. E. *et al.* Endosomal NOX2 oxidase exacerbates virus pathogenicity and is a target for antiviral therapy. *Nat. Commun.* **8**, (2017).
11. Docherty, A. B. *et al.* Features of 16,749 hospitalised UK patients with COVID-19 using the ISARIC WHO Clinical Characterisation Protocol. *medRxiv* **369**, 2020.04.23.20076042 (2020).
12. Alqahtani, J. S. *et al.* Prevalence, severity and mortality associated with COPD and smoking in patients with COVID-19: A rapid systematic review and meta-analysis. *PLoS ONE* **15**, e0233147 (2020).
13. Moisan, J. *et al.* TLR7 ligand prevents allergen-induced airway hyperresponsiveness and eosinophilia in allergic asthma by a MYD88-dependent and MK2-independent pathway. *AJP Lung Cell. Mol. Physiol.* **290**, L987–L995 (2006).
14. Pham Van, L. *et al.* Treatment with the TLR7 agonist R848 induces regulatory T-cell-

mediated suppression of established asthma symptoms. *Eur. J. Immunol.* **41**, 1992–1999 (2011).

15. Du, Q. *et al.* Imiquimod, a toll-like receptor 7 ligand, inhibits airway remodelling in a murine model of chronic asthma. *Clin. Exp. Pharmacol. Physiol.* **36**, 43–8 (2009).
16. Wang, X. *et al.* Prevention of airway inflammation with topical cream containing imiquimod and small interfering RNA for natriuretic peptide receptor. *Genet. Vaccines Ther.* **6**, 7 (2008).
17. Mortaz, E., Folkerts, G. & Redegeld, F. Mast cells and COPD. *Pulm. Pharmacol. Ther.* **24**, 367–72 (2011).
18. Bischoff, S. C. Role of mast cells in allergic and non-allergic immune responses: comparison of human and murine data. *Nat. Rev. Immunol.* **7**, 93–104 (2007).
19. Andersson, C. K., Mori, M., Bjermer, L., Löfdahl, C.-G. & Erjefält, J. S. Alterations in lung mast cell populations in patients with chronic obstructive pulmonary disease. *Am. J. Respir. Crit. Care Med.* **181**, 206–17 (2010).
20. Ballarin, A. *et al.* Mast cell infiltration discriminates between histopathological phenotypes of chronic obstructive pulmonary disease. *Am. J. Respir. Crit. Care Med.* **186**, 233–239 (2012).
21. Mortaz, E. *et al.* Cigarette smoke stimulates the production of chemokines in mast cells. *J. Leukoc. Biol.* **83**, 575–580 (2008).
22. Matsushima, H., Yamada, N., Matsue, H. & Shimada, S. TLR3-, TLR7-, and TLR9-mediated production of proinflammatory cytokines and chemokines from murine connective tissue type skin-derived mast cells but not from bone marrow-derived mast cells. *J. Immunol.* **173**, 531–541 (2004).
23. Yang, H. *et al.* Upregulation of Toll-like receptor (TLR) expression and release of cytokines from P815 mast cells by GM-CSF. *BMC Cell Biol.* **10**, 37 (2009).

490 24. Kulka, M., Alexopoulou, L., Flavell, R. A. & Metcalfe, D. D. Activation of mast cells by
491 double-stranded RNA: evidence for activation through Toll-like receptor 3. *J. Allergy Clin.*
492 *Immunol.* **114**, 174–182 (2004).
493 25. Beckett, E. L. *et al.* A new short-term mouse model of chronic obstructive pulmonary
494 disease identifies a role for mast cell tryptase in pathogenesis. *J. Allergy Clin. Immunol.*
495 **131**, 752–62 (2013).
496 26. Hansbro, P. M. *et al.* Importance of mast cell Prss31/transmembrane tryptase/tryptase-γ in
497 lung function and experimental chronic obstructive pulmonary disease and colitis. *J. Biol.*
498 *Chem.* **289**, 18214–27 (2014).
499 27. Jarnicki, A. G. *et al.* The inhibitor of semicarbazide-sensitive amine oxidase, PXS-4728A,
500 ameliorates key features of chronic obstructive pulmonary disease in a mouse model. *Br.*
501 *J. Pharmacol.* **173**, 3161–3175 (2016).
502 28. Fricker, M. *et al.* Chronic cigarette smoke exposure induces systemic hypoxia that drives
503 intestinal dysfunction. *JCI insight* **3**, (2018).
504 29. Tay, H. L. *et al.* Antagonism of miR-328 increases the antimicrobial function of
505 macrophages and neutrophils and rapid clearance of non-typeable Haemophilus influenzae
506 (NTHi) from infected lung. *PLoS Pathog.* **11**, e1004549 (2015).
507 30. Chen-Yu Hsu, A. *et al.* Targeting PI3K-p110α suppresses influenza virus infection in
508 chronic obstructive pulmonary disease. *Am. J. Respir. Crit. Care Med.* **191**, 1012–1023
509 (2015).
510 31. Franklin, B. S. *et al.* The adaptor ASC has extracellular and 'prionoid' activities that
511 propagate inflammation. *Nat. Immunol.* **15**, 727–37 (2014).
512 32. Fricker, M., Deane, A. & Hansbro, P. M. Animal models of chronic obstructive pulmonary
513 disease. *Expert Opin. Drug Discov.* **9**, 629–645 (2014).
514 33. Haw, T. J. *et al.* A pathogenic role for tumor necrosis factor-related apoptosis-inducing

ligand in chronic obstructive pulmonary disease. *Mucosal Immunol.* **9**, 859–72 (2016).

34. Liu, G. *et al.* Fibulin-1 regulates the pathogenesis of tissue remodeling in respiratory diseases. *JCI insight* **1**, 1–18 (2016).
35. Donovan, C. *et al.* Roles for T/B lymphocytes and ILC2s in experimental chronic obstructive pulmonary disease. *J. Leukoc. Biol.* **105**, 143–150 (2019).
36. Haw, T. J. *et al.* Toll-like receptor 2 and 4 have opposing roles in the pathogenesis of cigarette smoke-induced chronic obstructive pulmonary disease. *Am. J. Physiol. Lung Cell. Mol. Physiol.* **314**, L298–L317 (2018).
37. Starkey, M. R. *et al.* IL-22 and its receptors are increased in human and experimental COPD and contribute to pathogenesis. *Eur. Respir. J.* **54**, (2019).
38. Campbell, J. D. *et al.* A gene expression signature of emphysema-related lung destruction and its reversal by the tripeptide GHK. *Genome Med.* **4**, 67 (2012).
39. Christenson, S. A. *et al.* miR-638 regulates gene expression networks associated with emphysematous lung destruction. *Genome Med.* **5**, 114 (2013).
40. Tilley, A. E. *et al.* Down-regulation of the notch pathway in human airway epithelium in association with smoking and chronic obstructive pulmonary disease. *Am. J. Respir. Crit. Care Med.* **179**, 457–66 (2009).
41. Wortham, B. W., Eppert, B. L., Flury, J. L., Morgado Garcia, S. & Borchers, M. T. TLR and NKG2D signaling pathways mediate CS-induced pulmonary pathologies. *PLoS One* **8**, e78735 (2013).
42. Gantier, M. P. *et al.* TLR7 is involved in sequence-specific sensing of single-stranded RNAs in human macrophages. *J. Immunol.* **180**, 2117–24 (2008).
43. Kanno, A. *et al.* Targeting cell surface TLR7 for therapeutic intervention in autoimmune diseases. *Nat. Commun.* **6**, 6119 (2015).
44. Sin, D. D. *et al.* The effects of fluticasone with or without salmeterol on systemic

biomarkers of inflammation in chronic obstructive pulmonary disease. *Am. J. Respir. Crit. Care Med.* **177**, 1207–1214 (2008).

45. Weng, Z. *et al.* Quercetin is more effective than cromolyn in blocking human mast cell cytokine release and inhibits contact dermatitis and photosensitivity in humans. *PLoS One* **7**, e33805 (2012).
46. Huang, S.-W. *et al.* Imiquimod simultaneously induces autophagy and apoptosis in human basal cell carcinoma cells. *Br. J. Dermatol.* **163**, 310–20 (2010).
47. Drobits, B. *et al.* Imiquimod clears tumors in mice independent of adaptive immunity by converting pDCs into tumor-killing effector cells. *J. Clin. Invest.* **122**, 575–585 (2012).
48. Sohn, K.-C. *et al.* Imiquimod induces apoptosis of squamous cell carcinoma (SCC) cells via regulation of A20. *PLoS One* **9**, e95337 (2014).
49. Inglefield, J. R., Larson, C. J., Gibson, S. J., Lebrec, H. & Miller, R. L. Apoptotic responses in squamous carcinoma and epithelial cells to small-molecule toll-like receptor agonists evaluated with automated cytometry. *J. Biomol. Screen.* **11**, 575–85 (2006).
50. Meyer, T. *et al.* Induction of apoptosis by Toll-like receptor-7 agonist in tissue cultures. *Br. J. Dermatol.* **149**, 9–13 (2003).
51. Hogg, J. C., McDonough, J. E. & Suzuki, M. Small airway obstruction in COPD: New insights based on micro-CT imaging and MRI imaging. *Chest* **143**, 1436–1443 (2013).
52. Tisoncik, J. R. *et al.* Into the eye of the cytokine storm. *Microbiol. Mol. Biol. Rev.* **76**, 16–32 (2012).
53. Walsh, K. B. *et al.* Suppression of cytokine storm with a sphingosine analog provides protection against pathogenic influenza virus. *Proc Natl Acad Sci U S A* **108**, 12018–12023 (2011).
54. Teijaro, J. R., Walsh, K. B., Rice, S., Rosen, H. & Oldstone, M. B. Mapping the innate signaling cascade essential for cytokine storm during influenza virus infection. *Proc Natl*

565 *Acad Sci U S A* **111**, 3799–3804 (2014).
566 55. Gaschler, G. J. *et al.* Cigarette smoke exposure attenuates cytokine production by mouse
567 alveolar macrophages. *Am. J. Respir. Cell Mol. Biol.* **38**, 218–26 (2008).
568 56. van Zyl-Smit, R. N. *et al.* Cigarette smoke impairs cytokine responses and BCG
569 containment in alveolar macrophages. *Thorax* **69**, 363–370 (2014).
570 57. Berenson, C. S. *et al.* Impaired innate immune alveolar macrophage response and the
571 predilection for COPD exacerbations. *Thorax* 1–8 (2014). doi:10.1136/thoraxjnl-2013-
572 203669
573 58. Sethi, S. *et al.* Airway bacterial concentrations and exacerbations of chronic obstructive
574 pulmonary disease. *Am. J. Respir. Crit. Care Med.* **176**, 356–61 (2007).
575 59. Bauer, C. M. T. *et al.* Cigarette smoke suppresses type I interferon-mediated antiviral
576 immunity in lung fibroblast and epithelial cells. *J. Interferon Cytokine Res.* **28**, 167–79
577 (2008).
578 60. Modestou, M. A., Manzel, L. J., El-Mahdy, S. & Look, D. C. Inhibition of IFN-gamma-
579 dependent antiviral airway epithelial defense by cigarette smoke. *Respir. Res.* **11**, 64
580 (2010).
581 61. HuangFu, W.-C., Liu, J., Harty, R. N. & Fuchs, S. Y. Cigarette smoking products suppress
582 anti-viral effects of Type I interferon via phosphorylation-dependent downregulation of its
583 receptor. *FEBS Lett.* **582**, 3206–10 (2008).
584 62. Tian, X. *et al.* Poly I:C enhances susceptibility to secondary pulmonary infections by
585 gram-positive bacteria. *PLoS One* **7**, e41879 (2012).
586 63. Grine, L., Dejager, L., Libert, C. & Vandenbroucke, R. E. Dual inhibition of TNFR1 and
587 IFNAR1 in imiquimod-induced psoriasiform skin inflammation in mice. *J. Immunol.* **194**,
588 5094–102 (2015).
589 64. Puig, M. *et al.* TLR9 and TLR7 agonists mediate distinct type I IFN responses in humans

590 and nonhuman primates in vitro and in vivo. *J. Leukoc. Biol.* **91**, 147–58 (2012).
591 65. Sainathan, S. K. *et al.* Toll-like receptor-7 ligand imiquimod induces type I interferon and
592 antimicrobial peptides to ameliorate dextran sodium sulfate-induced acute colitis.
593 *Inflamm. Bowel Dis.* **18**, 955–967 (2012).
594 66. Budden, K. F. *et al.* Emerging pathogenic links between microbiota and the gut-lung axis.
595 *Nat. Rev. Microbiol.* **15**, 55–63 (2017).
596 67. Budden, K. F. *et al.* Functional effects of the microbiota in chronic respiratory disease.
597 *Lancet Respir. Med.* **7**, 907–920 (2019).
598 68. D.D., S. *et al.* The effects of fluticasone with or without salmeterol on systemic biomarkers
599 of inflammation in chronic obstructive pulmonary disease. *Am. J. Respir. Crit. Care Med.*
600 **177**, 1207–1214 (2008).
601 69. Hatchwell, L. *et al.* Toll-like receptor 7 governs interferon and inflammatory responses to
602 rhinovirus and is suppressed by IL-5-induced lung eosinophilia. *Thorax* **70**, thoraxjnl-
603 2014-205465 (2015).
604 70. Kanno, A. *et al.* Essential role for Toll-like receptor 7 (TLR7)-unique cysteines in an
605 intramolecular disulfide bond, proteolytic cleavage and RNA sensing. *Int. Immunol.* **25**,
606 413–22 (2013).
607 71. Collison, A. *et al.* The E3 ubiquitin ligase midline 1 promotes allergen and rhinovirus-
608 induced asthma by inhibiting protein phosphatase 2A activity. *Nat. Med.* **19**, 232–237
609 (2013).
610 72. Horvat, J. C. *et al.* Early-life chlamydial lung infection enhances allergic airways disease
611 through age-dependent differences in immunopathology. *J. Allergy Clin. Immunol.* **125**,
612 617–25, 625.e1-625.e6 (2010).
613 73. Starkey, M. R. *et al.* Constitutive production of IL-13 promotes early-life Chlamydia
614 respiratory infection and allergic airway disease. *Mucosal Immunol.* **6**, 569–579 (2013).

74. Starkey, M. R. *et al.* Tumor necrosis factor-related apoptosis-inducing ligand translates neonatal respiratory infection into chronic lung disease. *Mucosal Immunol.* **7**, 478–488 (2014).
75. Beckett, E. L. *et al.* TLR2, but not TLR4, is required for effective host defence against Chlamydia respiratory tract infection in early life. *PLoS One* **7**, e39460 (2012).
76. Essilfie, A.-T. *et al.* Macrolide therapy suppresses key features of experimental steroid-sensitive and steroid-insensitive asthma. *Thorax* **70**, 458–67 (2015).
77. Tao, Y. *et al.* The role of endogenous IFN-β in the regulation of Th17 responses in patients with relapsing-remitting multiple sclerosis. *J. Immunol.* **192**, 5610–5617 (2014).
78. Chen, G.-Y. *et al.* Simultaneous induction of autophagy and toll-like receptor signaling pathways by graphene oxide. *Biomaterials* **33**, 6559–6569 (2012).
79. Horvat, J. C. *et al.* Chlamydial respiratory infection during allergen sensitization drives neutrophilic allergic airways disease. *J. Immunol.* **184**, 4159–69 (2010).
80. Essilfie, A.-T. *et al.* Haemophilus influenzae infection drives IL-17-mediated neutrophilic allergic airways disease. *PLoS Pathog.* **7**, e1002244 (2011).
81. Horvat, J. C. *et al.* Neonatal chlamydial infection induces mixed T-cell responses that drive allergic airway disease. *Am. J. Respir. Crit. Care Med.* **176**, 556–64 (2007).
82. Eidelman, D. H., Ghezzo, H., Kim, W. D. & Cosio, M. G. The destructive index and early lung destruction in smokers. *Am. Rev. Respir. Dis.* **144**, 156–9 (1991).
83. Li, J. J. *et al.* IL-27/IFN-gamma induce MyD88-dependent steroid-resistant airway hyperresponsiveness by inhibiting glucocorticoid signaling in macrophages. *J Immunol* **185**, 4401–4409 (2010).

MAIN FIGURES

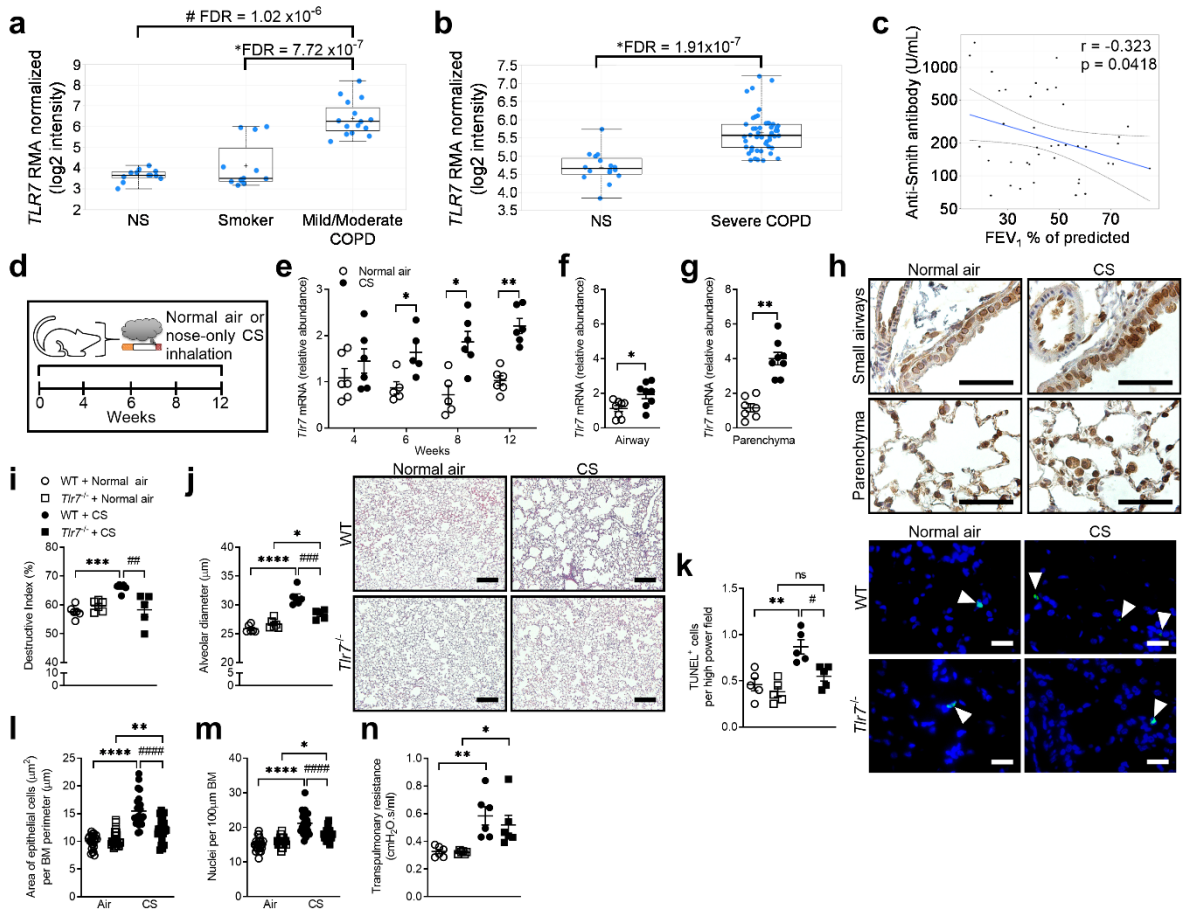

Figure 1 | TLR7 is increased in human and experimental COPD and promotes emphysema-like alveolar enlargement, airway remodeling and apoptosis in experimental COPD. (**a**) *TLR7* mRNA levels in airway epithelial brushings from non-smokers (NS), healthy smokers without COPD (Smoker) and COPD patients with Global Initiative for Chronic Obstructive Lung Disease (GOLD) stage I (mild) or II (moderate) disease (n = 12 NS; n = 12 Smokers; n = 15 mild or moderate COPD). (**b**) *TLR7* mRNA levels in lung parenchyma cores from NS and COPD patients with GOLD stage IV (severe) disease (n = 16 NS; n = 48 severe COPD). Differential gene expression analysis was performed using published microarray datasets (GEO accession numbers GSE5058 and GSE27597) and the numbers in panels **a** and **b** represent the false discovery rate (FDR), whereby * denotes FDR of COPD *vs.* NS; and #

650 denotes FDR of COPD *vs.* Smoker. (**c**) Correlation analysis of anti-Smith antibody levels in
651 serum and forced expiratory volume in 1 second (FEV_1) of mild-to-moderate COPD patients
652 (n = 40). (**d**) Induction of experimental COPD where wild-type (WT) mice were exposed to
653 nose-only inhalation of cigarette smoke (CS) for up to 12 weeks, controls received normal air.
654 (**e**) *Tlr7* mRNA levels in whole lungs of WT mice exposed to normal air or CS after 4, 6, 8 and
655 12 weeks (n = 6 mice per group). *Tlr7* mRNA levels in blunt-dissected (**f**) airways and (**g**) lung
656 parenchyma after 8 weeks of CS exposure (n = 6 mice per group). (**h**) Representative
657 micrographs (n = 3 mice per group) of TLR7 immunostaining in small airways (top) and lung
658 parenchyma (bottom) of WT mice exposed to normal air (left) or CS (right) for 8 weeks. Scale
659 bars, 50 μm. WT or TLR7-deficient ($Tlr7^{-/-}$) mice (n = 5-6 mice per group) were exposed to
660 normal air or CS for 8 weeks and alveolar enlargement was determined by (**i**) quantification of
661 destructive index and (**j**) mean linear intercept. Representative micrographs (right) of
662 hematoxylin and eosin-stained lung sections from WT (top panel) and $Tlr7^{-/-}$ (bottom panel)
663 mice exposed to normal air (left panel) or CS (right panel). Scale bars, 200 μm. (**k**)
664 Quantification of apoptotic cells (n = 5 mice per group) and representative micrographs (right)
665 of TUNEL-stained lung sections from WT (top panel) and $Tlr7^{-/-}$ (bottom panel) mice exposed
666 to normal air (left panel) or CS (right panel). Arrows indicate $TUNEL^+$ cells. Scale bars, 20
667 μm. (**l**) Quantification of small airway epithelial cell area per μm of basement membrane (BM)
668 perimeter and (**m**) nuclei numbers per 100 μm of BM perimeter of normal air- or CS-exposed
669 WT and $Tlr7^{-/-}$ mice (4 small airways per mouse, n = 6 mice per group). (**n**) Transpulmonary
670 resistance of normal air- or CS-exposed WT and $Tlr7^{-/-}$ mice (n = 5-6 mice per group). For
671 experimental studies, data are presented as means ± s.e.m. and are representative from two
672 independent experiments. For panels **e**, **f** and **g**, $*P < 0.05$; $**P < 0.01$ compared to normal air-
673 exposed controls using two-tailed Mann-Whitney test. For panels **i, j, k, l, m** and **n**, $*P < 0.05$;
674 $**P < 0.01$; $***P < 0.001$; $****P < 0.0001$ compared to normal air-exposed WT or $Tlr7^{-/-}$

675 controls, and $^{\#}P < 0.05$; $^{\#\#}P < 0.01$; $^{\#\#\#}P < 0.001$; $^{\#\#\#\#}P < 0.0001$ compared to CS-exposed WT
676 controls using one-way ANOVA with Bonferroni's multiple comparison test. ns, not
677 significant.

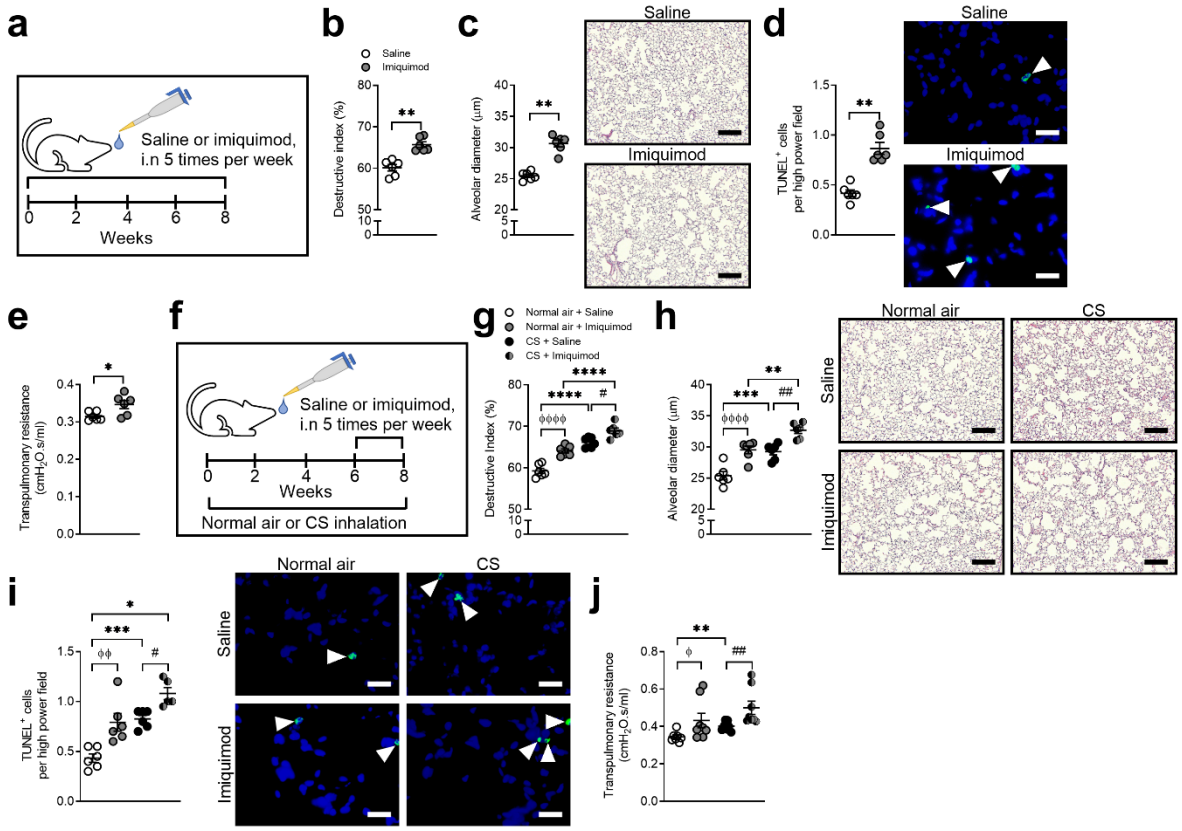

678

679 **Figure 2** | Pulmonary administration of the synthetic TLR7 agonist imiquimod induces
680 emphysema-like alveolar enlargement and apoptosis and impairs lung function in mice. (**a**)
681 Wild-type (WT) mice were administered imiquimod (50 µg in 50 µl sterile saline), intranasally
682 (i.n.) 5 times per week, for 8 weeks. Controls received sterile saline. (**b**) Quantification of
683 destructive index (n = 6 mice per group) of saline- or imiquimod-administered WT mice. (**c**)
684 Quantification of mean linear intercept (n = 6 mice per group) and representative micrographs
685 (right) of hematoxylin and eosin (H&E)-stained lung sections from saline (top panel)- or
686 imiquimod (bottom panel)-administered WT mice. Scale bars, 200 µm. (**d**) Quantification of
687 apoptotic cells (n = 6 mice per group) and representative micrographs (right) of TUNEL-
688 stained lung sections from saline (top panel)- or imiquimod (bottom panel)-administered WT
689 mice. Arrows indicate TUNEL$^+$ cells. Scale bars, 20 µm. (**e**) Transpulmonary resistance of
690 saline- or imiquimod-administered WT mice (n = 6 mice per group). (**f**) WT mice were exposed

to normal air or CS for 8 weeks and some groups were administered imiquimod (50 μg in 50 μl sterile saline), i.n. 5 times per week, between Week 6 to 8 (for 2 weeks). Controls received sterile saline. (**g**) Quantification of destructive index (n = 6 mice per group) of saline- or imiquimod-administered WT mice exposed to normal air or CS for 8 weeks. (**h**) Quantification of mean linear intercept (n = 6 mice per group) and representative micrographs (right) of H&E-stained lung sections from saline (top panel)- or imiquimod (bottom panel)-administered WT mice exposed to normal air (left panel) or CS (right panel) for 8 weeks. Scale bars, 200 μm. (**i**) Quantification of apoptotic cells (n = 6 mice per group) and representative micrographs (right) of TUNEL-stained lung sections from saline (top panel)- or imiquimod (bottom panel)-administered WT mice exposed to normal air (left panel) or CS (right panel) for 8 weeks. Arrows indicate $TUNEL^+$ cells. Scale bars, 20 μm. (**j**) Transpulmonary resistance of saline- or imiquimod-administered WT mice exposed to normal air or CS for 8 weeks (n = 8 mice per group). Throughout, data are presented as means ± s.e.m. and are representative of two independent experiments. For panels **b**, **c, d** and **e**, *p<0.05; **p<0.01 compared to normal air-exposed controls using two-tailed Mann-Whitney test. For panels **g**, **h**, **i**, and **j**, *$P < 0.05$; **$P < 0.01$; ***$P < 0.001$; ****$P < 0.0001$ compared to saline- or imiquimod-administered WT mice exposed to normal air, $^{\#}P < 0.05$; $^{\#\#}P < 0.01$ compared to saline-administered WT mice exposed to CS, and $^{\phi}P < 0.05$; $^{\phi\phi}P < 0.01$; $^{\phi\phi\phi\phi}P < 0.0001$ compared to saline-administered WT mice exposed to normal air by one-way ANOVA using Bonferroni's multiple comparison test.

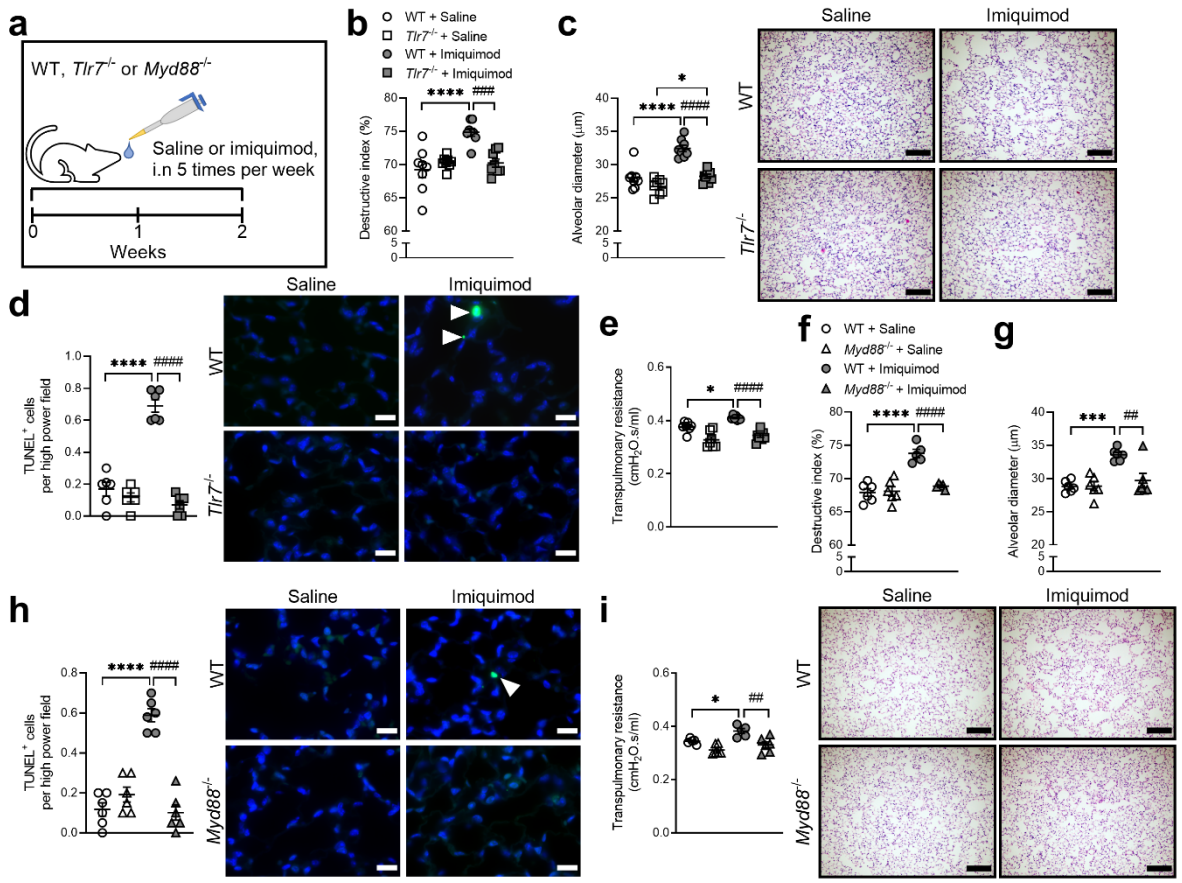

Figure 3 | Imiquimod induces emphysema in a TLR7- and MyD88-dependent manner. (**a**) Wild-type (WT) or TLR7-deficient (*Tlr7*$^{-/-}$) or MyD88-deficient (*Myd88*$^{-/-}$) mice were administered imiquimod (50 μg in 50 μl sterile saline), intranasally (i.n.) 5 times per week, for 2 weeks. Controls received sterile saline. (**b**) Quantification of destructive index (n = 8 mice per group) of saline- or imiquimod-administered WT and *Tlr7*$^{-/-}$ mice. (**c**) Quantification of mean linear intercept (n = 8 mice per group) and representative micrographs (right) of hematoxylin and eosin (H&E)-stained lung sections from WT (top panels) and *Tlr7*$^{-/-}$ (bottom panels) mice administered saline (left panels) or imiquimod (right panels). Scale bars, 200 μm. (**d**) Quantification of apoptotic cells (n = 6 mice per group) and representative micrographs (right) of TUNEL-stained lung sections from WT (top panels) and *Tlr7*$^{-/-}$ (bottom panels) mice administered saline (left panels) or imiquimod (right panels). Arrows indicate TUNEL^{+} cells. Scale bars, 20 μm. (**e**) Transpulmonary resistance of saline- or imiquimod-administered WT

723 and *Tlr7*$^{-/-}$ mice (n = 8 mice per group). (**f**) Quantification of destructive index (n = 6 mice per
724 group) of saline- or imiquimod-administered WT and *Myd88*$^{-/-}$ mice. (**g**) Quantification of
725 mean linear intercept (n = 6 mice per group) and representative micrographs (below) of H&E-
726 stained lung sections from WT (top panels) and *Myd88*$^{-/-}$ (bottom panels) mice administered
727 saline (left panels) or imiquimod (right panels). Scale bars, 200 μm. (**h**) Quantification of
728 apoptotic cells (n = 6 mice per group) and representative micrographs (right) of TUNEL-
729 stained lung sections from WT (top panels) and *Myd88*$^{-/-}$ (bottom panels) mice administered
730 saline (left panels) or imiquimod (right panels). Arrows indicate TUNEL^{+} cells. Scale bars, 20
731 μm. (**i**) Transpulmonary resistance of saline- or imiquimod-administered WT and *Myd88*$^{-/-}$
732 mice (n = 6 mice per group). Throughout, data are presented as means ± s.e.m. *$P < 0.05$; ***P
733 < 0.001; ***$P < 0.001$ compared to saline-administered WT, *Tlr7*$^{-/-}$ or *Myd88*$^{-/-}$ mice, and $^{\#}P <$
734 0.01; $^{\#\#\#}P < 0.01$; $^{\#\#\#\#}P < 0.0001$ compared to imiquimod-administered WT mice using one-
735 way ANOVA with Bonferroni's multiple comparison test.

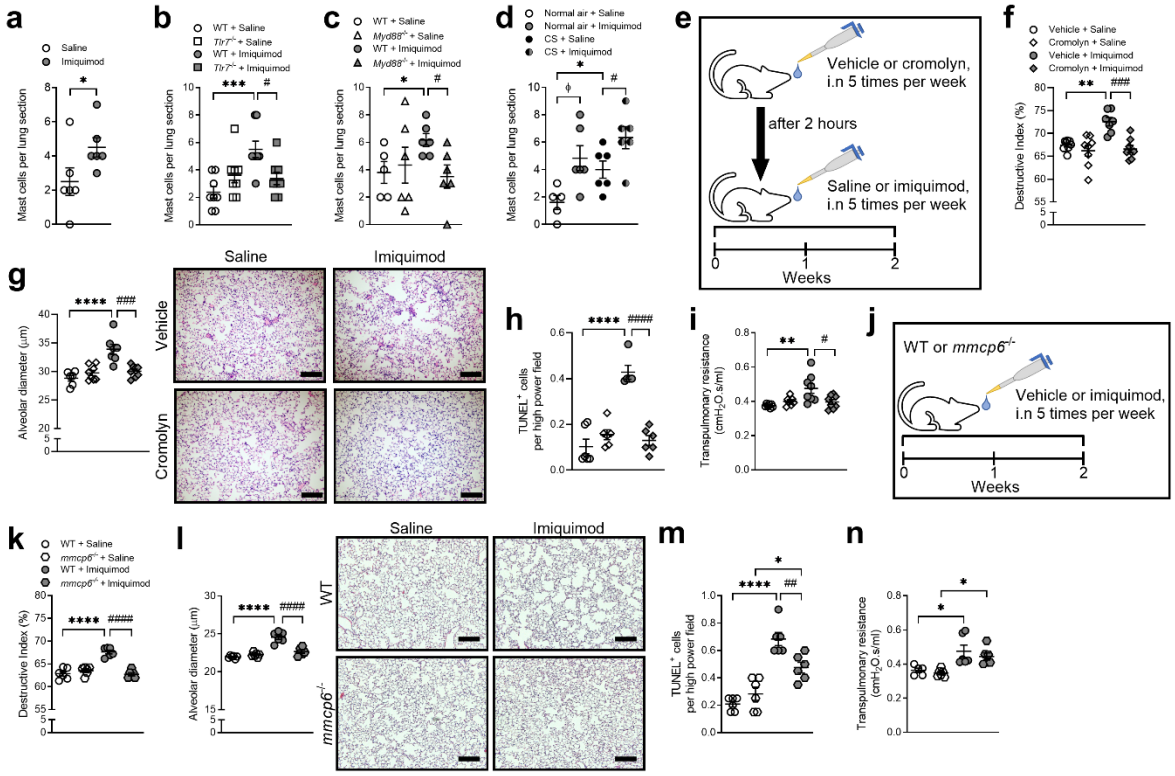

Figure 4 | Imiquimod induces pulmonary mast cell influx and imiquimod-induced emphysema is reduced in mice treated with the mast cell stabilizer cromolyn or deficient in the mast cell tryptase mMCP6. (**a**) Quantification of mast cells in lung sections from wild type (WT) mice (n = 6 mice per group) administered imiquimod or vehicle for 8 weeks. Quantification of mast cells in lung sections from (**b**) TLR7- (*Tlr7*$^{-/-}$) or (**c**) MyD88-deficient (*Myd88*$^{-/-}$) administered imiquimod or vehicle for 2 weeks (n = 8 mice per group). (**d**) Quantification of mast cells in lung sections from WT mice exposed to normal air or CS for 8 weeks and administered imiquimod or vehicle from Week 6 to 8. (**e**) Wild-type (WT) mice were first administered cromolyn (50 mg/kg body weight) or vehicle (sterile water), and after 2 hours, were administered imiquimod (50 μg) or vehicle. Cromolyn, imiquimod and vehicle were delivered intranasally (i.n.) 5 times per week, for 2 weeks. (**f**) Quantification of destructive index (n = 8 mice per group) of vehicle- or imiquimod-administered mice with or without cromolyn treatment. (**g**) Quantification of mean linear intercept (n = 8 mice per group) and representative

micrographs (right) of hematoxylin and eosin (H&E)-stained lung sections from vehicle (top panels) and cromolyn (bottom panels) mice administered vehicle (left panels) or imiquimod (right panels). Scale bars, 200 μm. (**h**) Quantification of apoptotic cells (n = 6 mice per group) and representative micrographs (right) of TUNEL-stained lung sections from vehicle (top panels) and cromolyn (bottom panels) mice administered with vehicle (left panels) or imiquimod (right panels). Arrows indicate $TUNEL^+$ cells. Scale bars, 20 μm. (**i**) Transpulmonary resistance of saline- or imiquimod-administered mice with or without cromolyn treatment (n = 8 mice per group). (**j**) WT or mouse mast cell protease-6-deficient ($mMCP6^{-/-}$) mice were administered imiquimod (50 μg in 50 μl) sterile saline, intranasally 5 times per week, for 2 weeks. Controls received sterile saline. (**k**) Quantification of destructive index (n = 6 mice per group) of saline- or imiquimod-administered WT and $mMCP6^{-/-}$ mice. (**l**) Quantification of mean linear intercept (n = 6 mice per group) and representative micrographs (right) of H&E-stained lung sections from WT (top panels) and $mMCP6^{-/-}$ (bottom panels) mice administered saline (left panels) or imiquimod (right panels). Scale bars, 200 μm. (**m**) Quantification of apoptotic cells (n = 6 mice per group) and representative micrographs (right) of TUNEL-stained lung sections from WT (top panels) and $mMCP6^{-/-}$ (bottom panels) mice administered saline (left panels) or imiquimod (right panels). Arrows indicate $TUNEL^+$ cells. Scale bars, 20 μm. (**n**) Transpulmonary resistance of saline- or imiquimod-administered WT and $mMCP6^{-/-}$ mice (n = 6 mice per group). Throughout, data are presented as means ± s.e.m. $^*P < 0.05$; $^{**}P < 0.01$; $^{***}P < 0.001$; $^{****}P < 0.0001$ compared to vehicle/saline-administered WT or $mMCP6^{-/-}$ mice, and $^{\#}P < 0.05$; $^{\#\#}P < 0.01$; $^{\#\#\#}P < 0.001$; $^{\#\#\#\#}P < 0.0001$ compared to imiquimod-administered WT mice, and $\phi P < 0.05$ compared to saline-administered WT mice exposed to normal air using one-way ANOVA using Bonferroni's multiple comparison test.

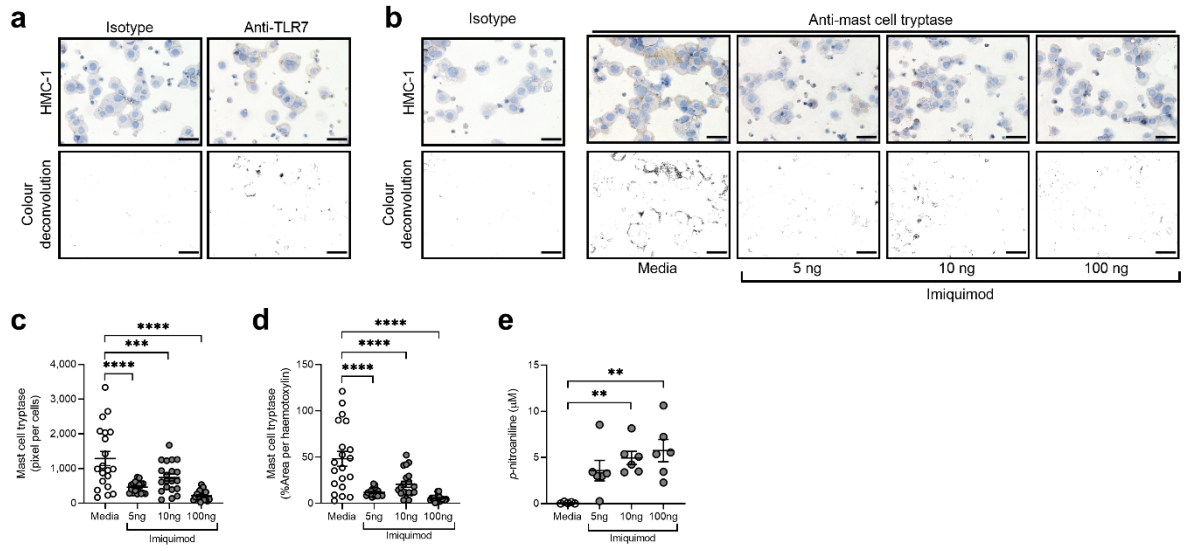

773

774 **Figure 5** | Imiquimod induces the release of mast cell tryptase from human mast cells. (**a**)
775 Representative micrographs (top panels, n = 3) and color deconvolution (bottom panels) of
776 isotype control (left panels) and TLR7 (right panels) immunostaining of HMC-1 human mast
777 cells. Scale bars, 50 μm. (**b**) Representative micrographs (top panels, n = 3) and color
778 deconvolution (bottom panels) of isotype control (left panel) and mast cell tryptase (right
779 panels) immunostaining of HMC-1 cells incubated with media or imiquimod (5, 10 or 100 ng)
780 for 1 hour. Quantification of mast cell tryptase in cells (10 random fields per sample, n = 3 per
781 group) normalized to (**c**) number of cells or (**d**) area of hematoxylin of HMC-1 cells incubated
782 with media or imiquimod (5, 10 or 100 ng) for 1 hour. (**e**) Quantification of mast cell tryptase
783 activity (n = 6 per group) in terms of p-nitroaniline levels in culture supernatants from HMC-
784 1 cells incubated with media or imiquimod (5, 10 or 100 ng) for 1 hour. Throughout, data are
785 presented as means ± s.e.m. $^{**}P < 0.01$; $^{***}P < 0.001$; $^{****}P < 0.0001$ compared to HMC-1
786 cells incubated with media using one-way ANOVA with Bonferroni's multiple comparison
787 test.

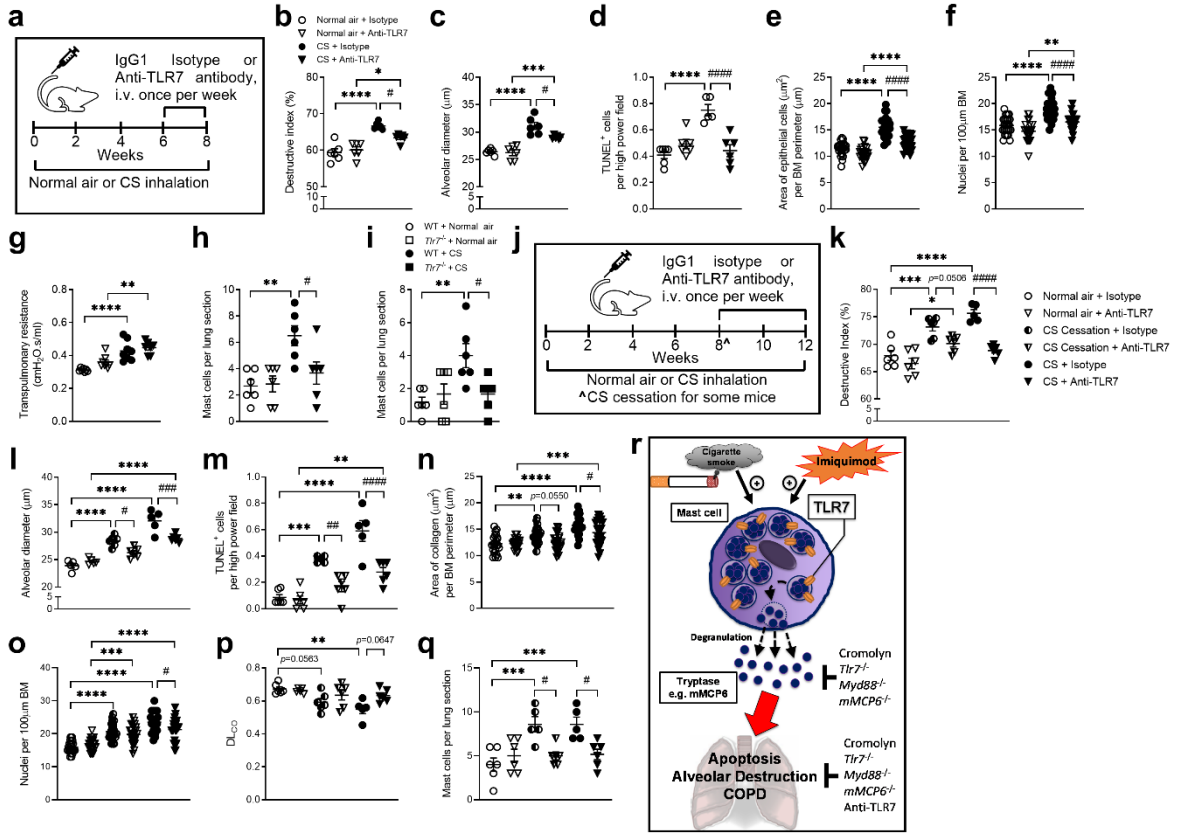

788

789 **Figure 6** | Therapeutic treatment with anti-TLR7 monoclonal antibody reduces CS-induced
790 emphysema and mast cell influx in experimental COPD. (**a**) Wild-type (WT) mice were
791 exposed to normal air or CS for 8 weeks and treated with neutralizing anti-TLR7 monoclonal
792 antibody or isotype control, intravenously (i.v.) once per week for 2 weeks, between Week 6
793 to 8. (**b**) Quantification of destructive index (*n* = 6 mice per group) in lungs of isotype- or anti-
794 TLR7-treated WT mice exposed to normal air or CS for 8 weeks. (**c**) Quantification of mean
795 linear intercept (*n* = 6 mice per group) of isotype or anti-TLR7 -treated WT mice exposed to
796 normal air or CS for 8 weeks. (**d**) Quantification of apoptotic cells (*n* = 6 mice per group) in
797 TUNEL-stained lung sections from isotype or anti-TLR7 treated WT mice exposed to normal
798 air or CS for 8 weeks. Quantification of (**e**) small airway epithelial cell area per μm of basement
799 membrane (BM) perimeter and (**f**) nuclei numbers per 100 μm of BM perimeter of isotype- or
800 anti-TLR7-treated WT mice exposed to normal air or CS for 8 weeks (4 small airways per

mouse, n = 6 mice per group). (**g**) Transpulmonary resistance of isotype- or anti-TLR7-treated WT mice exposed to normal air or CS for 8 weeks (n = 6 mice per group). (**h**) Quantification of mast cells in lung sections from isotype- or anti-TLR7-treated WT mice exposed to normal air or CS for 8 weeks (n = 6 mice per group). (**i**) Quantification of mast cells in lung sections from WT and *Tlr7*$^{-/-}$ mice exposed to normal air or CS for 8 weeks (n = 6 mice per group). (**j**) WT mice were exposed to normal air or CS for 12 weeks and treated with neutralizing anti-TLR7 monoclonal antibody or isotype control, i.v. once per week, between Week 8 to 12 (for 4 weeks). Some mice had CS cessation others continued CS exposure after 8 weeks prior to anti-TLR7 treatment. (**k**) Quantification of destructive index, (**l**) mean linear intercept and (**m**) apoptotic cells (n = 5-6 mice per group) in lungs of isotype- or anti-TLR7-treated WT mice exposed to normal air or CS with CS cessation or continued CS exposure from 8-12 weeks. Quantification of (**n**) small airway epithelial cell area per μm of basement membrane (BM) perimeter and (**o**) nuclei numbers per 100 μm of BM perimeter of isotype- or anti-TLR7-treated WT mice exposed to normal air or CS with CS cessation or continued CS exposure from 8-12 weeks (4 small airways per mouse, n = 5-6 mice per group). (**p**) Measurement of diffusing lung capacity for carbon monoxide (DL_{CO}) of isotype- or anti-TLR7-treated WT mice exposed to normal air or CS with CS cessation or continued CS exposure from 8-12 weeks (n = 5-6 mice per group). (**q**) Quantification of mast cells in lung sections from isotype- or anti-TLR7-treated WT mice exposed to normal air or CS with CS cessation or continued CS exposure from 8-12 weeks (n = 5-6 mice per group). (**r**) Schematic representation of proposed mechanisms of how TLR7 contributes to CS-induced apoptosis and emphysema-like alveolar enlargement in experimental COPD in a mast cell-specific tryptase-dependent manner. Throughout, data are presented as means ± s.e.m. *$P < 0.05$; **$P < 0.01$; ***$P < 0.001$; ****$P < 0.0001$; compared to isotype- or anti-TLR7-administered WT mice exposed to normal air, and $^{\#}P < 0.05$; $^{\#\#}P <$

825 0.01; $^{\#\#\#}P < 0.001$; $^{\#\#\#\#}P < 0.0001$ compared to isotype-administered WT mice exposed to CS

826 by one-way ANOVA using Bonferroni's multiple comparison test.

827 **ONLINE METHODS**

828 **Ethics statement.** This study was performed in accordance with the recommendations issued
829 in the Australian code of practice for the care and use of animals for scientific purposes by the
830 National Health and Medical Research Council of Australia. All protocols were approved by
831 the Animal Ethics Committee of The University of Newcastle, Australia.

832

833 **Microarray analysis of differential human gene expression.** Differential gene expression
834 analysis of published datasets (Gene Expression Omnibus [GEO] accession numbers GSE5058
835 and GSE27597)[38–40] was performed using Array Studio software (Omicsoft Corporation,
836 Research Triangle Park, NC) from a general linear model adjusting for age and gender and the
837 Benjamini–Hochberg method for *P*-value adjustment as described previously[33,38–40].

838

839 **Endogenous RNA quantification.** The amount of anti-Smith antibody, was quantified using
840 anti-Sm/RNP-C (IgG) enzyme-linked immunosorbent assay (ELISA, 35-SNRHU-E01,
841 ALPCO Diagnostics, Salem, NH) in the serum of patients with clinically diagnosed COPD
842 from the Advair Biomarkers in COPD (ABC) trial study (**Supplementary Table 1**)[68]. Serum
843 anti-Smith antibody levels were then tested for correlation with lung function (forced
844 expiratory volume in 1 second, FEV_1 % predicted). Study participants were diagnosed as
845 having COPD based on an average smoking of 10 pack-years and post-bronchodilator FEV_1:
846 forced vital capacity (FVC) ratio of less than 70%. Participants were randomly selected and
847 stratified by quantiles of FEV_1. Samples were run in duplicate and the coefficient of variance
848 (CV) determined. The dynamic range was 0-300 U/mL and analytical sensitivity of the kit was
849 1.0 U/mL. The Advair clinical trial was registered with
850 www.clinicaltrials.gov (NCT00120978).

851

852 **Animals.** Female, 7-8-week-old, wild-type (WT) controls, Toll-like receptor (TLR)7-deficient
853 (*Tlr7*$^{-/-}$) BALB/c mice[69], mouse mast cell protease-6-deficient (*mmcp6*$^{-/-}$) C57BL/6 mice[25] and
854 protease serine member S31-deficient (*Prss31*$^{-/-}$) C57BL/6 mice[26] were from obtained from
855 Australian BioResources facility (Moss Vale, NSW, Australia). All animals were housed in the
856 BioResources Facility at the Hunter Medical Research Institute (New Lambton Heights, NSW,
857 Australia) and kept under a 12-hour light and dark cycle. Animals had free access to sterile
858 food and water. Cages were chosen at random for treatments with or without exposure to
859 normal air or cigarette smoke (CS). Power was not explicitly calculated for each experiment.
860 Numbers of mice were typically used based on knowledge from prior experiments and
861 publications. CS exposure of mice was performed by research technicians who were blinded
862 to the study.
863
864 **Murine model of experimental COPD.** Age- and sex-matched 7-8-week-old mice were
865 randomly exposed to normal air or CS *via* the nose only for up to 12 weeks as extensively
866 described previously[25–37]. Briefly, mice were simultaneously exposed to CS (twelve 3R4F
867 reference cigarettes, University of Kentucky, Lexington, KY, twice per day, 5 times per week,
868 for up to 12 weeks) using a custom-designed and purpose-built nose-only, directed flow
869 inhalation and smoke-exposure system (CH Technologies, Westwood, NJ) housed in a
870 biosafety cabinet. Each exposure typically lasted for 75 minutes.
871
872 ***In vivo* activation of TLR7.** Some mice were administered 50 μg of TLR7 agonist imiquimod
873 (clone R837, Invivogen, San Diego, CA) in 50 μl sterile Dulbecco's phosphate-buffered saline
874 (PBS, Life Technologies, Mulgrave, Victoria, Australia)[62], intranasally (i.n) under isoflurane-
875 induced anesthesia, 5 times per week, either for 2 or 8 weeks in the absence of CS exposure or
876 between weeks 6-8 of CS exposure. Controls received sterile saline.

***In vivo* mast cell stabilization.** Some mice were administered 50 mg/kg of body weight of cromolyn sodium salt[45] (C0399, >95% purity, Sigma Aldrich/Merck, Castle Hill, New South Wales, Australia) in 50 µl sterile ultrapure water, intranasally (i.n) under isoflurane-induced anesthesia, 5 times per week, for up to 2 weeks. Controls received sterile saline.

***In vivo* neutralization of TLR7 with monoclonal antibody.** Some mice were administered neutralizing anti-TLR7 (clone Ba/F3; 4 mg/kg of body weight) monoclonal antibody or IgG1/κ isotype control[43,70], by intravenous (i.v) injection under isoflurane-induced anesthesia, once per week, during the last 2 weeks (between weeks 6-8) or 4 weeks (between weeks 8-12) of continued CS exposure or CS cessation.

Isolation of RNA. Total RNA was extracted from whole lung tissue or blunt-dissected airways and parenchyma as described previously[33,71]. Briefly, the trachea and lungs were excised, and the airways carefully separated from the lung parenchyma with sterile forceps. Whole lungs, airways and parenchyma were then snap frozen and stored at -80°C. Tissues were thawed and homogenized in 500 µL of sterile PBS (Life Technologies, Mulgrave, Victoria, Australia) using a Tissue-Tearor stick homogenizer (BioSpec Products, Bartesville, OK) on ice. Total RNA was extracted using TRIzol reagent (Invitrogen, Mount Waverly, Victoria, Australia) according to manufacturer's instructions and stored at -80°C[25,33].

Real-time quantitative polymerase chain reaction (qPCR). Total RNA from whole lungs, airways and parenchyma (1,000 ng) were reversed-transcribed using Bioscript reverse transcriptase (Bioline, Alexandria, New South Wales, Australia) and random hexamer primers (Invitrogen) as described previously[25,26,33,72–76]. The mRNA levels of cytokines, chemokines,

COPD-related factors and interferon-related factors were determined by qPCR (ABIPrism7000, Applied Biosystems, Scoresby, Victoria, Australia). Assays were performed using SYBR Green Supermix (KAPA Biosystems Inc., Wilmington, MA), normalized to the house-keeping hypoxanthine-guanine phosphoribosyltransferase (*Hprt*) transcript and expressed as relative abundance to normal air-exposed WT controls. Custom designed primers (Integrated DNA Technologies, Baulkham Hills, New South Wales, Australia) were used (**Supplementary Table 2**).

Immunohistochemistry. Lungs were perfused, inflated, formalin-fixed, paraffin-embedded and sectioned (4-6 μm). Longitudinal sections of the left lung were kept on a heating block at 70°C for 15 minutes, rehydrated through a series of xylene (2x) and ethanol gradient (2x absolute, 90%, 80%, 70%, 50%, 0.85% saline and PBS) washes, followed by antigen retrieval with citrate buffer (10 mM citric acid, 0.05% Tween 20, pH 6.0) in a steam cooker for 30 minutes. Sections were blocked with casein blocker (Thermo Scientific) at room temperature for 1 hour. Sections were then washed with PBS (5x, 5 minutes each) and incubated with primary anti-TLR7 rabbit antibody[77,78] (ab45371, Abcam, Melbourne, Victoria, Australia) overnight at 4°C, washed with PBS (5x, 5 minutes each), followed by anti-rabbit horseradish peroxidase-conjugated secondary antibody incubation at 37°C for 30 minutes (R&D Systems, Gymea, New South Wales, Australia) as per manufacturer's recommendations. The 3,3'-diaminobenzidine chromogen-substrate buffer (DAKO, North Sydney, New South Wales, Australia) was applied to sections and incubated in the dark at room temperature for ~12 minutes. Sections were washed in PBS (5x, 5 minutes each), counterstained with hematoxylin (5 minutes), dehydrated, mounted and analyzed with a BX51 microscope (Olympus, Tokyo, Shinjuku, Japan) and Image-Pro Plus software (Media Cybernetics, Rockville, MD).

Airway and parenchymal inflammation. Airway inflammation was assessed by differential enumeration of inflammatory cells in cytospin preparations from bronchoalveolar lavage fluid (BALF) as described previously[25,33,76,79,80]. Briefly, BALF was collected by two 500 µl lung lavages with Hank's Balanced Salt Solution (Life Technologies) through a cannula inserted into the trachea. BALF was centrifuged (527 xg, 8 minutes, 4°C using Heraeus Multifuge X3 Centrifuge with TX-1000 Swinging Bucket Rotor [ThermoFisher Scientific, Scoresby Victoria, Australia]), the resulting supernatant collected, and red blood cells were lysed using lysis buffer (1 ml, Tris-buffered NH_4Cl). Lysis buffer was then diluted with approximately 3 ml of Hank's Balanced Salt Solution (Life Technologies) and centrifuged. Resultant supernatant was then decanted, and cell pellets re-suspended in Hank's Balanced Salt Solution. Total leukocytes were determined using a hemocytometer. Cells were cytocentrifuged and stained with May-Grunwald-Giemsa. Differential leukocyte counts were enumerated according to morphological criteria (250 cells by light microscopy using a BX51 microscope, Olympus, at 40x magnification)[25,33,76,79,80]. All slides were coded, and counts performed in a blinded manner.

Histopathology. Histopathology was assessed at 10x and 40x magnification in longitudinal lung sections stained with hematoxylin and eosin (H&E) and scored based on a set of custom-designed criteria as described previously[26,81]. Slides were coded and assessments performed in a blinded manner.

Airway remodeling. Longitudinal sections of the left single-lobe lung were stained with H&E. Airway epithelial area (μm^2) and cell (nuclei) number were assessed at 40x or 100x magnification, quantified from a minimum of 3 small airways per lung section from each mouse using ImageJ software (Version 1.50, NIH, New York City, NY) and normalized to

basement membrane (BM) perimeter (μm) as described previously[25,26,33]. Slides were coded and quantifications performed in a blinded manner.

Alveolar enlargement. Longitudinal sections (4-6 μm thick) of the left single-lobe lung were stained with H&E to assess alveolar septal damage using the destructive index[82], and alveolar size and diameter using the mean linear intercept technique, respectively[25,30,33]. Briefly, 40 randomized images of lung sections at 40x magnification were taken using the BX51 microscope (Olympus) and Image-Pro Plus software (Media Cybernetics). Images with partial lung sections (the edge of lung section) or that contained multiple airways, blood vessels and areas of inflammation and fibrosis were excluded from the counts. Ten viable images were then superimposed with destructive index or mean linear intercept grids using ImageJ software (Version 1.50, NIH), and counts were made in a blinded manner and averaged per lung section for each mouse[25,30,33].

Apoptosis. Longitudinal sections of the left single-lobe lung were stained with terminal deoxynucleotidyl transferase dUTP nick end labeling (TUNEL) assay kits (Promega, Sydney, New South Wales, Australia) according to the manufacturer's instructions. Apoptosis in lung parenchyma was assessed by enumerating the numbers of $TUNEL^+$ cells in 20 randomized, high-powered fields (fluorescent microscopy using the BX51 microscope [Olympus] at 100x magnification) in a blinded fashion and averaged per lung section for each mouse[33]. Cells were defined as apoptotic when superimposed images of cells stained with TUNEL (green) overlapped with nuclei stained with Bisbenzimide H 33342 (blue, Sigma Aldrich/Merck). $TUNEL^+$ inflammatory cells or cells in alveolar spaces were excluded from the counts (verified by light microscopy using the BX51 microscope [Olympus], 100x magnification)[33].

977 **Lung Function.** Mice were anesthetized with ketamine (117 mg/kg) and xylazine (14.4 mg/kg,
978 Troy Laboratories, Smithfield, Australia) prior to tracheostomy. Tracheas were then cannulated
979 with a 19-gauge catheter, and a single-breath maneuver to assess the diffusing lung capacity
980 for carbon monoxide (DL_{CO}) was performed[28]. Briefly, lungs were inflated with 0.7 mL of
981 tracer gas mixture (0.318% Ne, 0.302% CO, balance was air). Following a 9-second breath
982 hold, 0.7 mL of gas was withdrawn from the lung, diluted to 2 mL (total volume) with room
983 air, and the concentrations of Ne and CO were measured by gas chromatography (60-second
984 gas analysis time; Micro GC Fusion® Gas Analyzer, INFICON, Singapore). The DF_{CO} is
985 expressed as a value between 0 and 1; complete uptake of CO is equal to 1, and no uptake of
986 CO is equal to 0. After that, the cannulated tracheas were attached to FlexiVent apparatus (FX1
987 System; SCIREQ, Montreal, Canada). Transpulmonary resistance was assessed (tidal volume
988 of 8 ml/kg at a respiratory rate of 450 breaths/minutes)[25]. The anesthetic combination and
989 ventilation pattern are commonly used and recommended by the manufacturer[25,79,83].
990 Assessments were performed at least three times and the average calculated for each mouse.
991
992 **Enumeration of mast cells in lung tissue.** Longitudinal sections of the left single-lobed lung
993 were stained with toluidine blue and the number of mast cells were enumerated in a blinded
994 fashion (light microscopy using the BX51 microscope [Olympus] at 20x or 40x magnification)
995 and represented as number of mast cells per lung section for each mouse[25,26].
996
997 **Human mast cell culture.** Cells of the human mast cell line (HMC)-1 were cultured in
998 Dulbecco's modified Eagle medium (DMEM, D5671, Sigma Aldrich/Merck) containing 10%
999 fetal bovine serum (Bovogen), 25 mmol HEPES buffer, 100 U/ml penicillin, and 100 µg/ml
1000 streptomycin (37°C, 5% CO_2). HMC-1 cells were seeded at 500,000 cells per well and
1001 stimulated with imiquimod (5, 10 or 100 ng, Invivogen) in 50 µl DMEM supplemented with

0.5% fetal bovine serum or medium only (control) for 1 hour. Cells were centrifuged (234 x*g*, 5 minutes, room temperature [Heraeus Multifuge X3 Centrifuge]) and resulting supernatants were collected. Cell pellets were then resuspended in 150 µL DMEM, cytocentrifuged and air-dried overnight prior to immunocytochemistry.

TLR7 and mast cell tryptase immunocytochemistry. Cells were fixed with methanol (-20°C, 15 minutes) and blocked with 1% bovine serum albumin (Sigma Aldrich/Merck) at room temperature for 1 hour. Sections were then washed with PBS (5x, 5 minutes each) and incubated with primary anti-TLR7 rabbit antibody (Abcam) or anti-mast cell tryptase antibody (ab2378, Abcam) overnight at 4°C, washed with PBS (5x, 5 minutes each), followed by anti-rabbit (R&D Systems, Gymea, New South Wales, Australia) or anti-mouse (ab97023, Abcam) horseradish peroxidase-conjugated secondary antibody incubation at 37°C for 1 hour as per manufacturer's recommendations. The DAKO buffer was applied to sections which were incubated in the dark at room temperature for ~12 minutes. Sections were washed in PBS (5x, 5 minutes each), counterstained with hematoxylin (5 minutes), air-dried and mounted. Twenty randomized images at 40x magnification were taken per slide using the BX51 microscope and Image-Pro Plus software. For quantification of mast cell tryptase, 10 viable images (x40) were randomly selected and the numbers of HMC-1 cells were enumerated in each image. DAB chromogen and hematoxylin signals were then separated and converted into pixels using the ImageJ Color Deconvolution plugin (NIH). DAB signal was quantified as the area (pixels) normalized to the number of HMC-1 cells in the image. In addition, DAB signal is also presented as percentage area of hematoxylin-stained area of HMC-1 cells.

Human mast cell tryptase activity. Mast cell tryptase activity in culture supernatant was determined using mast cell degranulation assay kits (Chemicon, Merck). Briefly, culture

supernatants (20 µl) from HMC-1 cells incubated with media or imiquimod (5, 10 or 100 ng) were mixed with assay buffer (160 µL) and labelled substrate tosyl-gly-pro-lys-*p*NA (20 µl). Samples were incubated for 1 hour at 37°C. The chromophore *p*-nitroaniline (*p*NA) is cleaved from the labelled substrate by mast cell tryptase in the sample. Remaining free *p*NA is then determined using a microtiter plate reader (SpectraMax M5, Molecular Devices, CA, USA) at 405nm. Optical density values were obtained, compared to known concentrations of a *p*NA standard curve and relative mast cell tryptase activities were defined.

Statistical analyses. Data are presented as means ± standard error of the mean (s.e.m.) from at least two independent experiments. Mean values appeared to be normally distributed and appropriate statistical tests were performed for each figure. The variance between the groups that were compared statistically appeared to be similar. Comparisons between two groups were assessed using the two-tailed Mann-Whitney test. Comparisons between multiple groups were made using one-way ANOVA with Bonferroni's multiple comparison test. Correlation analyses were made using Spearman's rank correlation coefficient test. *P* values were calculated, and minimum statistical significance was accepted at $P < 0.05$. Early death was used as an exclusion criterion for animal experiments. However, no animals died in any of the experimental protocols. Significant outliers were identified using Grubb's test and excluded from statistical analyses. All statistical analyses were performed using GraphPad Prism Software version 8 (San Diego, CA).

SUPPLEMENTARY MATERIAL

SUPPLEMENTARY RESULTS

CS-induced small airway remodeling is reduced in *Tlr7*$^{-/-}$ mice

There was no significant difference in small airway epithelial cell area (thickening, **Supplementary Fig. 1a**) between normal air-exposed WT (top left panel) and *Tlr7*$^{-/-}$ (bottom left panel) mice. Both CS-exposed WT (top right panel) and *Tlr7*$^{-/-}$ (bottom right panel) mice had increased small airway epithelial cell thickening compared to their respective normal air-exposed controls (top and bottom left panels). However, CS-exposed *Tlr7*$^{-/-}$ mice (bottom right panel) had reduced small airway epithelial cell thickening compared to CS-exposed WT controls (top right panel). This was associated with reduced nuclei numbers (**Supplementary Fig. 1b**) in CS-exposed *Tlr7*$^{-/-}$ (bottom right panel) compared to CS-exposed WT controls (top right panel).

CS-induced pulmonary inflammation is unaltered in *Tlr7*$^{-/-}$ mice

We assessed whether TLR7 plays a role in CS-induced inflammation. CS exposure of WT mice increased total leukocytes, macrophages, neutrophils and lymphocytes in BALF compared to normal air-exposed WT and *Tlr7*$^{-/-}$ controls, respectively (**Supplementary Fig. 2a-d**). These cells were similarly increased in CS-exposed *Tlr7*$^{-/-}$ mice compared to normal air-exposed *Tlr7*$^{-/-}$ controls. The levels of these inflammatory cells were not different between CS-exposed WT and *Tlr7*$^{-/-}$ mice.

Next, histopathology in lung tissue was assessed[1,2]. CS exposure of WT mice increased histopathology score, characterized by increased total, airway, vascular and parenchymal inflammation (**Supplementary Figure 2e–i**). CS-exposed *Tlr7*$^{-/-}$ mice also had increases in

1071 these histopathology scores compared to normal air-exposed *Tlr7*$^{-/-}$ controls and were not
1072 different to CS-exposed WT controls.

1073 We also profiled mRNA levels of pro-inflammatory cytokines, chemokines and COPD-
1074 related factors in lung homogenates (**Supplementary Fig. 2j-t**). These factors were all
1075 increased in CS-exposed WT and *Tlr7*$^{-/-}$ mice compared to normal air-exposed WT and *Tlr7*$^{-/-}$
1076 controls, respectively, and were not different between CS-exposed WT and *Tlr7*$^{-/-}$ mice.

1077 Given that TLR7 mediates anti-viral interferon responses[3–5] and these responses are
1078 suppressed in COPD patients[6–11], we also interferon beta (*Ifnb*), interferon gamma (*Ifng*),
1079 interferon lambda (*Ifnl*) and interferon receptor 1 (*Ifnar1*) mRNA levels (**Supplementary Fig.**
1080 **2u-y**). CS exposure of both WT and *Tlr7*$^{-/-}$ mice reduced the mRNA levels of *Ifna*, *Ifnb*, *Ifng*,
1081 *Ifnl* and *Ifnar1* compared to normal air-exposed WT and *Tlr7*$^{-/-}$ controls, respectively. *Ifng*
1082 mRNA levels were not altered by CS exposure. The mRNA levels of these interferons were
1083 not different between CS-exposed WT and *Tlr7*$^{-/-}$ mice.

1084

1085 **Imiquimod had no effect on pulmonary inflammation or small airway remodelling**

1086 We next assessed the effects of chronic (8 weeks) administration of imiquimod on pulmonary
1087 inflammation and small airway remodelling in mice. Imiquimod did not have any effect on the
1088 numbers of inflammatory cells in BALF (**Supplementary Fig. 3a-d**), histopathology scores
1089 (**Supplementary Fig. 3e-i**), small airway epithelial cell thickening (**Supplementary Fig. 3j**)
1090 or nuclei numbers (**Supplementary Fig. 3k**), or interferon-related mRNA levels
1091 (**Supplementary Fig. 3l-p**).

1092

1093 **Imiquimod had minimal effects on CS-induced pulmonary inflammation and small**
1094 **airway remodelling**

CS exposure of mice for 8 weeks with saline- or imiquimod-administration in the last 2 weeks increased total leukocytes, macrophage, neutrophils and lymphocytes in BALF compared to normal air-exposed saline- or imiquimod-administered controls, respectively (**Supplementary Fig. 4a-d**). The levels of these inflammatory cells were not significantly altered between CS-exposed saline- or imiquimod-administered mice.

CS exposure of saline- or imiquimod-administered mice also led to increased total histopathology, airway, vascular and parenchymal inflammation scores when compared to saline- and imiquimod-administered normal air-exposed controls respectively, (**Supplementary Figure 4e–i**). These were not significantly altered between CS-exposed saline- or imiquimod-administered mice.

CS exposure of saline- or imiquimod-administered mice also led to increases in small airway epithelial cell thickening and nuclei numbers compared to normal air-exposed saline- and imiquimod-administered controls, respectively (**Supplementary Fig. 4j and k**). These were not significantly different between CS-exposed saline- or imiquimod-administered mice.

Interferon-related mRNAs were largely suppressed in saline-administered CS-exposed mice compared to saline-administered normal air-exposed controls (**Supplementary Fig. 4l-p**). Imiquimod, restored *Ifna* mRNA levels in CS-exposed mice (**Supplementary Fig. 4l**) but did not affect *Ifnb*, *Ifng*, *Ifnl* or *Ifnar1* mRNA levels in normal air- or CS-exposed mice (**Supplementary Fig. 4m-p**).

Imiquimod had no effect on pulmonary inflammation or small airway remodeling in *Tlr7*$^{-/-}$ and *Myd88*$^{-/-}$ mice

We next examined the impact of imiquimod alone for 2 weeks on pulmonary inflammation and small airway remodelling in *Tlr7*$^{-/-}$ mice. Imiquimod did not alter the numbers of inflammatory cells in BALF (**Supplementary Fig. 5a-d**), histopathology scores (**Supplementary Fig. 5e-i**),

small airway epithelial cell thickening (**Supplementary Fig. 5j**) or nuclei numbers (**Supplementary Fig. 5k**), or interferon-related mRNA levels (**Supplementary Fig. 5l-o**) in WT or *Tlr7*$^{-/-}$ mice.

Consistent with the observations in *Tlr7*$^{-/-}$ mice, imiquimod also did not alter the numbers of inflammatory cells in BALF (**Supplementary Fig. 6a-d**), histopathology scores (**Supplementary Fig. 6e-i**), small airway epithelial cell thickening (**Supplementary Fig. 6j**) or nuclei numbers (**Supplementary Fig. 6k**), or interferon-related mRNA levels (**Supplementary Fig. 6l-o**) in WT or *Myd88*$^{-/-}$ mice.

Imiquimod-induced apoptosis is reduced by administration of cromolyn

Administration of saline had no significant effect on the level of TUNEL^{+} cells (**Supplementary Fig. 7**) in lung parenchyma of vehicle (top left panel)- or cromolyn (bottom left panel)-administered mice. In contrast, administration of imiquimod increased the levels of TUNEL^{+} cells in vehicle-administered mice (top right panel), but not in those treated with cromolyn (bottom right panel) compared to their respective saline-administered controls (top and bottom left panels). Notably, imiquimod-induced TUNEL^{+} cells were significantly reduced in cromolyn- (bottom right panel) compared to vehicle-treated controls (top right panel).

Mast cell stabilizer cromolyn with or without imiquimod did not alter pulmonary inflammation or small airway remodeling

We assessed the impact of the mast cell stabilizer cromolyn on pulmonary inflammation and small airway remodelling in mice administered saline or imiquimod. Treatment with cromolyn with or without imiquimod had no effects on the numbers of inflammatory cells in BALF (**Supplementary Fig. 8a-d**), histopathology scores (**Supplementary Fig. 8e-i**), small airway

epithelial cell thickening (**Supplementary Fig. 8j**) or nuclei numbers (**Supplementary Fig. 8k**).

Imiquimod-induced apoptosis is reduced in *mmcp6*$^{-/-}$ mice

To assess the relationship between TLR7 and mast cell granule-specific tryptase, WT or *mmcp6*$^{-/-}$ mice were administered either saline or imiquimod i.n for 2 weeks. Administration of saline had no effect on the levels of TUNEL^{+} cells (**Supplementary Fig. 9**) in lung parenchyma between WT (top left panel) and *mmcp6*$^{-/-}$ (bottom left panel) mice. Administration of imiquimod increased the levels of TUNEL^{+} cells in WT (top right panel) but not *mmcp6*$^{-/-}$ mice (bottom right panel) compared to their respective saline-administered controls (top and bottom left panels). Notably, imiquimod-induced TUNEL^{+} cells were significantly reduced in *mmcp6*$^{-/-}$ mice (bottom right panel) compared to WT controls (top right panel).

Imiquimod had no effect on pulmonary inflammation or small airway remodeling in *mmcp6*$^{-/-}$ mice

Consistent with our other observations, imiquimod did not alter the numbers of inflammatory cells in BALF (**Supplementary Fig. 10a-d**), histopathology scores (**Supplementary Fig. 10e-i**), or small airway epithelial cell thickening (**Supplementary Fig. 10j**) or nuclei numbers (**Supplementary Fig. 10k**) in WT or *mmcp6*$^{-/-}$ mice.

Imiquimod-induced emphysema is not altered in *Prss31*$^{-/-}$ mice

Imiquimod appeared to induce alveolar septal damage and enlargement in WT and *Prss31*$^{-/-}$ mice when compared to their respective saline-administered controls although this was not statistically significant (**Supplementary Fig. 11a and b**). Imiquimod-induced alveolar septal

damage and enlargement was not different in *Prss31*$^{-/-}$ compared to imiquimod-administered WT controls.

Imiquimod did not induce other known proteases in the lungs of mice

We also assessed whether imiquimod-induced emphysema was mediated through other known proteases in the lungs. We determined the levels of neutrophil elastase, myeloperoxidase and total matrix metalloproteinase (MMP) activity in lung homogenates from mice administered saline or imiquimod for 8 weeks (**Supplementary Fig. 12a-c**). Imiquimod did not alter the activity levels of these proteases in the lung of mice.

Prophylactic neutralization of TLR7 prevents CS-induced experimental COPD/emphysema

There was no significant different in alveolar diameter (**Supplementary Fig. 13a**) between normal air-exposed mice treated with isotype (top left panel)- or anti-TLR7 (bottom left panel) antibodies. CS exposure increased alveolar diameter in isotype-treated mice (top right panel), compared to their respective normal air-exposed controls (top and bottom left panels). Notably, anti-TLR7-treated CS-exposed mice (bottom right panel) had reduced alveolar diameter compared to isotype-treated CS-exposed controls (top right panel). This was associated with reduced numbers of TUNEL^{+} cells (**Supplementary Fig. 13b**) in the parenchyma of anti-TLR7-treated CS-exposed mice (bottom right panel) compared to isotype-treated CS-exposed controls (top right panel).

Next, we assessed the impact of TLR7 neutralization on CS-induced small airway remodeling. CS exposure increased small airway epithelial cell thickening in isotype-treated mice (top right panel), but not those treated with Anti-TLR7 (bottom right panel) compared to their respective normal air-exposed controls (top and bottom left panels) (**Supplementary Fig.**

13c). Notably, anti-TLR7-treated CS-exposed mice (bottom right panel) had reduced small airway epithelial cell thickening compared to isotype-treated CS-exposed controls (top right panel). This was associated with reduced nuclei numbers (**Supplementary Fig. 13d**) in the parenchyma of anti-TLR7-treated CS-exposed (bottom right panel) compared to isotype-treated CS-exposed (top right panel) controls.

Prophylactic neutralization of TLR7 had minimal effects on CS-induced pulmonary inflammation

We determined the impact of neutralizing TLR7 with a monoclonal antibody on pulmonary inflammation. CS exposure increased the numbers of leukocytes, macrophages, neutrophils and lymphocytes in BALF from mice administered isotype control antibodies (**Supplementary Fig. 14a-d**). Anti-TLR7 antibodies suppressed the CS exposure-induced increases in total leukocytes and macrophages but not neutrophils or lymphocytes (**Supplementary Fig. 14a-d**). This may be due to the suppression of BALF macrophages (**Supplementary Fig. 14b**).

CS exposure increased histopathology scores, characterized by increased total, airway, vascular and parenchymal inflammation in mice compared to normal air-exposed controls, which were not altered by administration of either isotype or anti-TLR7 (**Supplementary Figure 14e–i**). These scores were not altered in CS-exposed mice treated with anti-TLR7 compared to CS-exposed isotype controls.

Interferon-related mRNA levels was either not altered or was suppressed in CS-exposed mice treated with either isotype or anti-TLR7 antibodies compared to their normal air-exposed controls (**Supplementary Figure 14j–n**). Interestingly, anti-TLR7 appeared to restore *Ifna* mRNA levels in CS-exposed mice (**Supplementary Fig. 14j**) but did not affect *Ifnb*, *Ifng*, *Ifnl* or *Ifnar1* mRNA levels in normal air- or CS-exposed mice (**Supplementary Fig. 14l-n**).

Therapeutic anti-TLR7 treatment suppresses CS-induced emphysema and small airway remodeling

We then assessed the impact of therapeutically targeting TLR7 with anti-TLR7 monoclonal antibody on CS-induced emphysema and small airway remodeling. There was no significant difference in alveolar diameter (**Supplementary Fig. 15a**) between normal air-exposed mice treated with isotype (top left panel)- or anti-TLR7 (bottom left panel) antibodies. Both CS cessation (top middle panel) and continually CS-exposed (top right panel) mice treated with isotype antibodies had increased alveolar diameter compared to normal air-exposed mice treated with isotype antibodies (top left panel). In contrast, there was no significant difference in alveolar diameter in CS cessation (bottom middle panel) and continually CS-exposed (bottom right panel) mice treated with anti-TLR7 antibodies compared to air-exposed mice treated with anti-TLR7 antibodies (bottom left panel). Importantly, anti-TLR7 treatment reduced alveolar diameter in CS cessation (bottom middle panel) and continually CS-exposed (bottom right panel) mice compared to their respective isotype treated counterparts (top middle and top right panels).

There was no significant difference in small airway epithelial cell thickening (**Supplementary Fig. 15b**) between normal air-exposed mice treated with isotype (top left panel)- or anti-TLR7 (bottom left panel) antibodies. Both CS cessation (top middle panel) and continually CS-exposed (top right panel) mice treated with isotype antibodies had increased small airway epithelial cell thickening compared to air-exposed mice treated with isotype antibodies (top left panel). In contrast, there was no significant difference in small airway epithelial cell thickening in CS cessation (bottom middle panel) and continually CS-exposed (bottom right panel) mice treated with anti-TLR7 antibodies compared to air-exposed mice treated with anti-TLR7 antibodies (bottom left panel). Importantly, anti-TLR7 treatment reduced small airway epithelial cell thickening in CS cessation (bottom middle panel) and

continually CS-exposed (bottom right panel) mice compared to their respective isotype treated counterparts (top middle and top right panels).

Therapeutic treatment with anti-TLR7 monoclonal antibody had modest effects on CS-induced pulmonary inflammation

We then assessed the therapeutic potential of anti-TLR7 neutralizing antibody on pulmonary inflammation and small airway remodelling. The numbers of total leukocytes, macrophages, neutrophils and lymphocytes in BALF were largely not significantly increased in mice that were exposed to CS for 8 weeks and then underwent CS cessation and isotype or anti-TLR7 treatment from 8-12 weeks compared to normal air exposed isotype- or anti-TLR7 treated controls (**Supplementary Fig. 16a-d**). However, these cells were substantially increased in mice exposed to continually CS for 12 weeks and treated with isotype from weeks 8-12. Notably, the levels of all inflammatory cells were reduced in continually CS-exposed mice treated with anti-TLR7 compared to treatment with isotype controls.

Both CS cessation and continually CS-exposed mice treated with isotype had increased histopathology scores, characterized by increased total, airway, vascular and parenchymal inflammation compared to their normal air-exposed counterparts (**Supplementary Figure 16e–i**). Anti-TLR7 treatment, did not alter these histopathology scores in CS cessation or continually CS-exposed mice.

Supplementary Table 1. Correlation analysis of serum anti-Smith antibody and lung function in human COPD

Patient	Age	Gender	Smoking status	FEV_1 % predicted	Average anti-Smith antibody (U/mL)	CV
1	63	F	Ex	31.29274	133.9	1.4
2	63	M	Cur	57.67217	92.6	8.9
3	75	M	Ex	85.05295	117.4	2.9
4	58	M	Ex	42.03528	158.2	2.3
5	73	M	Cur	57.46761	85.6	2.3
6	64	M	Cur	60.0486	68.2	1.0
7	69	F	Ex	56.38084	66.3	1.9
8	58	F	Ex	38.43131	127.9	2.2
9	61	M	Cur	41.33902	183.0	3.3
10	71	F	Ex	72.70775	198.7	3.4
11	74	F	Cur	76.54096	285.8	3.0
12	67	M	Cur	73.1108	228.4	7.2
13	66	M	Cur	26.76206	610.6	8.4
14	68	M	Ex	17.2032	1694.9	7.7
15	63	M	Ex	45.3973	626.4	0.2
16	81	F	Ex	38.80983	539.2	2.6

17	71	M	Ex	48.73073	653.9	4.1
18	60	F	Cur	49.66636	191.7	5.1
19	71	F	Ex	37.57592	131.9	9.1
20	70	M	Ex	40.93218	718.7	0.1
21	55	F	Cur	19.11071	186.0	3.7
22	70	M	Ex	22.56967	138.7	2.7
23	76	M	Ex	40.20005	278.5	8.4
24	66	M	Ex	23.49932	66.0	18.3
25	57	F	Cur	28.40203	302.6	1.5
26	51	M	Cur	23.88658	913.5	0.3
27	88	F	Ex	70.81437	129.1	2.1
28	69	M	Ex	40.13399	86.6	1.1
29	79	M	Ex	60.27518	185.8	4.3
30	67	F	Cur	52.44526	192.2	1.5
31	75	M	Ex	48.08761	146.3	0.3
32	62	M	Ex	31.09317	81.4	3.6
33	73	M	Ex	34.85255	76.2	2.6
34	75	M	Ex	29.19837	625.0	1.7
35	80	F	Ex	57.19733	187.8	4.2

36	61	M	Cur	51.56451	457.1	3.8
37	76	M	Ex	15.33453	1286.9	3.8
38	59	F	Ex	48.96422	1227.2	1.0
39	76	F	Ex	46.91628	188.6	27.5
40	50	M	Cur	68.95058	130.5	3.9

Abbreviations: FEV_1, forced expiratory volume in 1 second; CV, coefficient of variance; M, male; F, female; Ex, ex-smoker; Cur, current smoker

Supplementary Table 2. Custom-designed primers used in qPCR analysis

Primer	**Primer sequence (5' → 3')**
Tlr7 forward	AGTGCCTGAAAAATGCCCTG
Tlr7 reverse	GCTCTCTGAAGAATGTCACCAC
Tnf-α forward	TCTGTCTACTGAACTTCGGGGTGA
Tnf-α reverse	TTGTCTTTGAGATCCATGCCGTT
Cxcl1 forward	GCTGGGATTCACCTCAAGAA
Cxcl1 reverse	CTTGGGGACACCTTTTAGCA
Ccl2 forward	TGAGTAGCAGCAGGTGAGTGGGG
Ccl2 reverse	TGTTCACAGTTGCCGGCTGGAG
Ccl3 forward	CTCCCAGCCAGGTGTCATTTT
Ccl3 reverse	CTTGGACCCAGGTCTCTTTGG
Ccl8 forward	GGGCCCAATGCATCCACATGC
Ccl8 reverse	TTCAGCGCAGACTTACATGCCC
Ccl12 forward	CCGGGAGCTGTGATCTTCA
Ccl12 reverse	AACCCACTTCTCGGGGT
Ccl20 forward	CGACTGTTGCCTCTCGTACA
Ccl20 reverse	AGGAGGTTCACAGCCCTTTT
Ccl22 forward	TGGCTACCCTGCGTCGTGTCCCA
Ccl22 reverse	CGTGATGGCAGAGGGTGACGG
Il-33 forward	CCTCCCTGAGTACATACAATGACC
Il-33 reverse	GTAGTAGCACCTGGTCTTGCTCTT
Mmp12 forward	CCTCGATGTGGAGTGCCCGA
Mmp12 reverse	CCTCACGCTTCATGTCCGGAG

Saa3 forward	TGATCCTGGGAGTTGACAGCCAA
Saa3 reverse	ACCCCTCCGGGCAGCATCATA
Ifna forward	SAWCYCTCCYAGACTCMTTCTGCA
Ifna reverse	TATDTCCTCACAGCCAGCAG
Ifnb forward	CCCTATGGAGATGACGGAGA
Ifnb reverse	ACCCAGTGCTGGAGAAATTG
*Ifn*g forward	GAGGAACTGGCAAAAGG
Ifng reverse	TTGCTGATGGCCTGATTGTC
Ifnl forward	CTTCAGGCCACAGCAGAGCCCAAG
Ifnl reverse	ACACACTTGAGGTCCCGGAGGA
Ifnar1 forward	CTGTGTCATGTGTGCTTCCC
Ifnar1 reverse	ATCTTTCCGTGTGCTCCTCA
Hprt forward	AGGCCAGACTTTGTTGGATTTGAA
Hprt reverse	CAACTTGCGCTCATCTTAGGATTT

1269

1270

SUPPLEMENTARY FIGURES

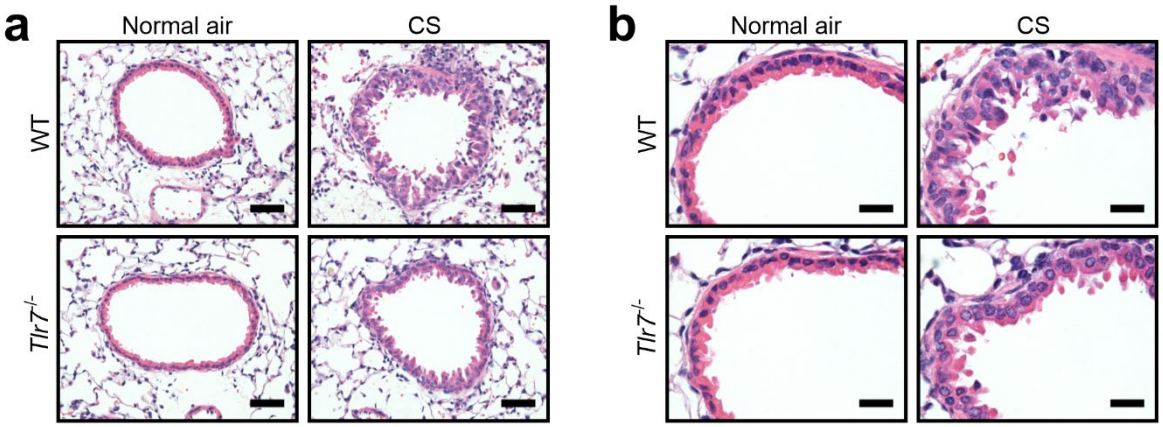

Supplementary Figure 1 | CS-induced small airway epithelial thickening is reduced in *Tlr7*$^{-/-}$ mice. WT or *Tlr7*$^{-/-}$ mice were exposed to normal air or CS for 8 weeks. (**a**) Representative micrographs of small airways in H&E-stained lung sections (n = 6 mice per group) from WT (top panels) and *Tlr7*$^{-/-}$ (bottom panels) mice exposed to normal air (left panels) or CS (right panels) for 8 weeks. Scale bars, 50 µm. (**b**) Representative micrographs showing small airway epithelial cell nuclei in H&E-stained lung sections (n = 6 mice per group) from WT (top panels) and *Tlr7*$^{-/-}$ (bottom panels) mice exposed to normal air (left panels) or CS (right panels) for 8 weeks. Scale bars, 20 µm.

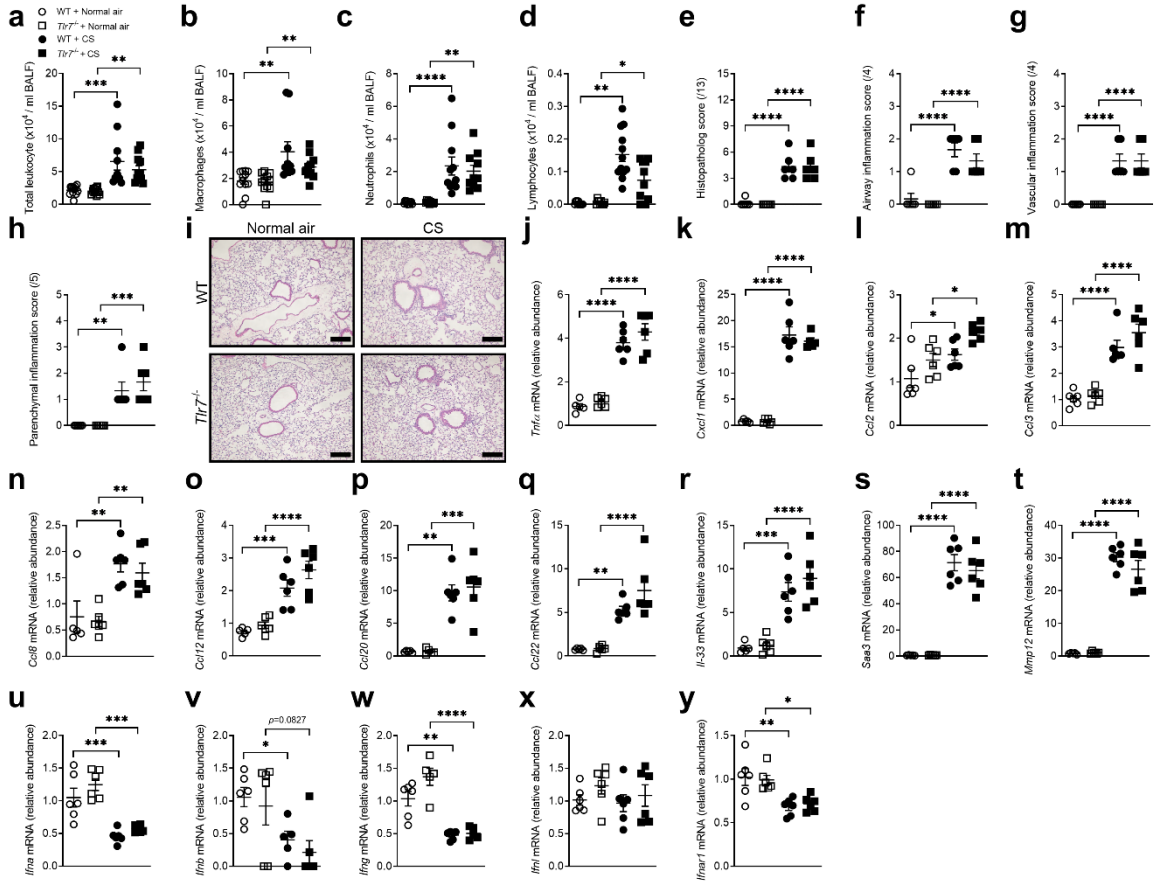

Supplementary Figure 2 | CS-induced pulmonary inflammation is unaltered in *Tlr7*$^{-/-}$ mice. WT or *Tlr7*$^{-/-}$ mice were exposed to normal air or CS for 8 weeks. (**a**) Total leukocytes, (**b**) macrophages, (**c**) neutrophils and (**d**) lymphocytes in May-Grunwald Giemsa stained BALF cytospins from WT or *Tlr7*$^{-/-}$ mice exposed to normal air- or CS for 8 weeks (n = 6 mice per group). (**e – h**) Histopathology scores and (**i**) representative micrographs of H&E-stained lung sections (n = 6 mice per group) from WT (top panels) and *Tlr7*$^{-/-}$ (bottom panels) mice exposed to normal air (left panels) or CS (right panels) for 8 weeks. Scale bars, 200 µm. (**j**) Tumour necrosis factor (*Tnf*)-α, (**k**) chemokine (C-X-C motif) ligand (*Cxcl*)1, (**l**) chemokine (C-C motif) ligand (*Ccl*)2, (**m**) *Ccl3*, (**n**) *Ccl8*, (**o**) *Ccl12*, (**p**) *Ccl20*, (**q**) *Ccl22*, (**r**) interleukin (*Il*)-33, (**s**) serum amyloid A3 (*Saa3*), (**t**) matrix metalloproteinase (*Mmp*)12, (**u**) interferon alpha (*Ifna*), (**v**) interferon beta (*Ifnb*), (**w**) interferon gamma (*Ifng*), (**x**) interferon lambda (*Ifnl*) and (**y**) interferon receptor 1 (*Ifnar1*) mRNA levels in whole lung homogenates by qPCR from WT

or *Tlr7*$^{-/-}$ mice exposed to normal air- or CS for 8 weeks (n = 6 mice per group). mRNA data were normalized to the house-keeping *Hprt* transcript and expressed as relative abundance to normal air-exposed WT controls. All data are presented as means ± s.e.m. *P< 0.05; **P< 0.01; ***P< 0.001; ****P< 0.0001 compared to normal air-exposed WT or *Tlr7*$^{-/-}$ controls by one-way ANOVA with Bonferonni's multiple comparison test.

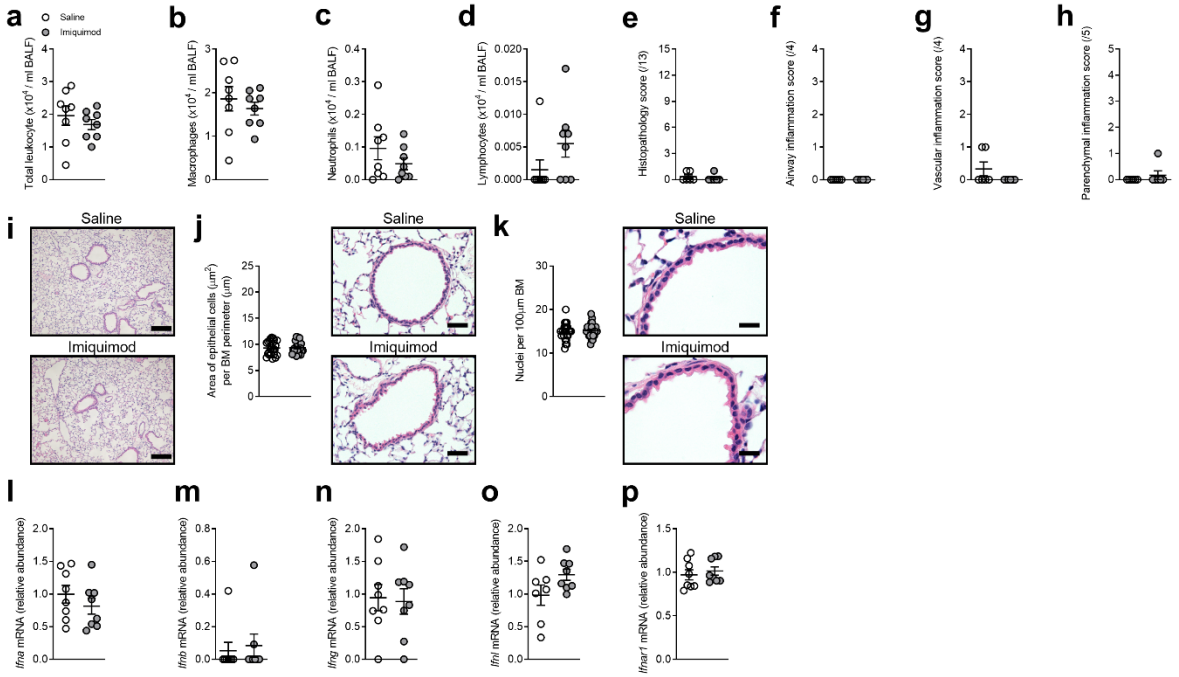

Supplementary Figure 3 | Administration of imiquimod had no effect on pulmonary inflammation or small airway remodelling in mice. WT mice were administered imiquimod (50 μg) in sterile saline, intranasally 5 times per week, for 8 weeks. Controls received sterile saline. (**a**) Total leukocytes, (**b**) macrophages, (**c**) neutrophils and (**d**) lymphocytes in May-Grunwald Giemsa stained BALF cytospins from WT mice administered saline or imiquimod (*n* = 8 mice per group). (**e – h**) Histopathology scores and (**i**) representative micrographs of small airways in H&E-stained lung sections (*n* = 6 mice per group) from WT mice administered saline (top panel) and imiquimod (bottom panel). Scale bars, 200 μm. (**j**) Quantification of small airway epithelial cell area per BM perimeter (4 small airways per mouse, *n* = 6 mice per group) and representative micrographs (right panels) of small airways in H&E-stained lung sections from WT mice administered saline (top panel) and imiquimod (bottom panel). Scale bars, 50 μm. (**k**) Quantification of nuclei numbers per 100 μm of BM perimeter (4 small airways per mouse, *n* = 6 mice per group) and representative micrographs (right panels) showing small airway epithelial cell nuclei in H&E-stained lung sections from WT mice administered saline (top panel) and imiquimod (bottom panel). Scale bars, 20 μm. (**l**) *Ifna*, (**m**)

Ifnb, (**n**) *Ifng*, (**o**) *Ifnl* and (**p**) *Ifnar1* mRNA levels in whole lung homogenates by qPCR from WT mice administered saline or imiquimod (n = 8 mice per group). mRNA data were normalized to the house-keeping *Hprt* transcript and expressed as relative abundance to saline-administered WT controls. All data are presented as means ± s.e.m.

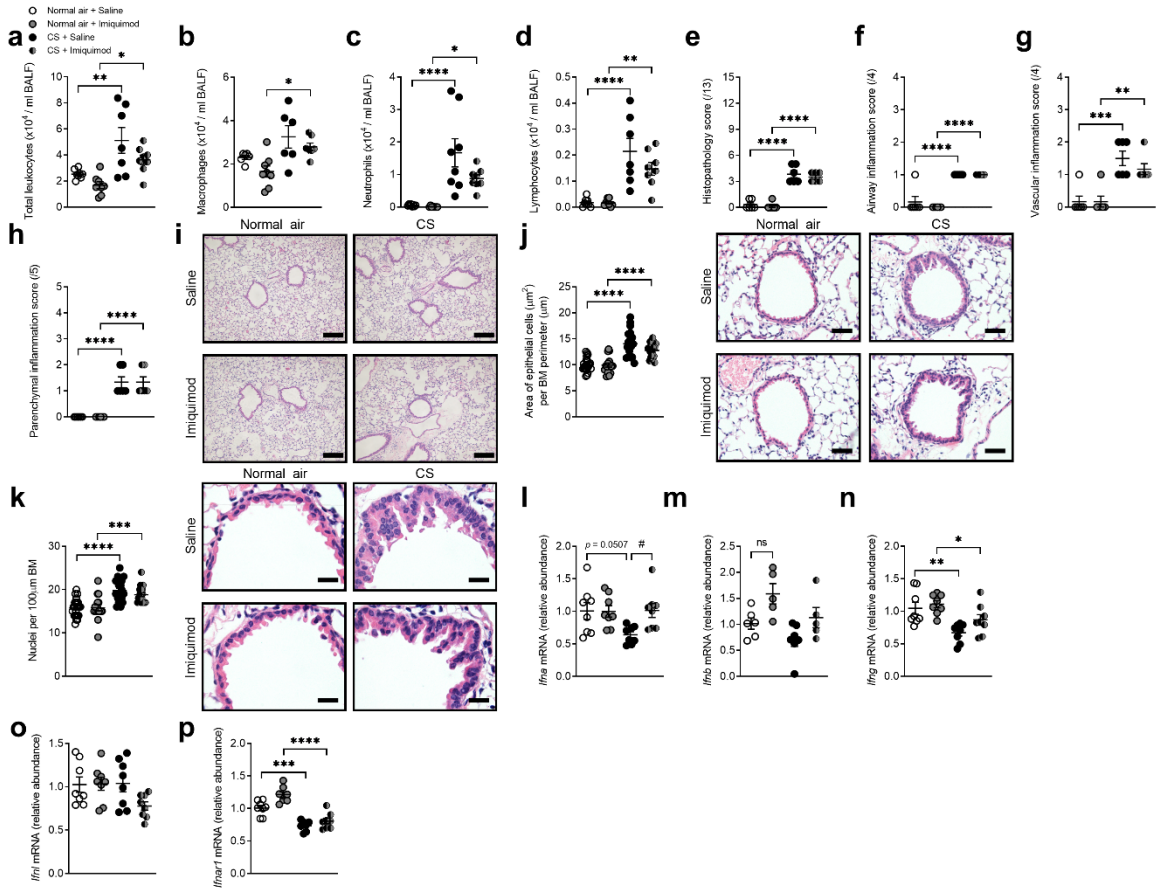

Supplementary Figure 4 | Administration of imiquimod during chronic CS exposure has minimal effects on pulmonary inflammation or small airway remodelling in experimental COPD. WT mice were exposed to normal air or CS for 8 weeks and were administered imiquimod (50 µg) in sterile saline intranasally 5 times per week, between Week 6 to 8 (for 2 weeks). Controls received sterile saline. (**a**) Total leukocytes, (**b**) macrophages, (**c**) neutrophils and (**d**) lymphocytes in May-Grunwald Giemsa stained BALF cytospins from saline- and imiquimod-administered WT mice exposed to normal air or CS for 8 weeks (n = 8 mice per group). (**e – h**) Histopathology scores and (**i**) representative micrographs of H&E-stained lung sections (n = 6 mice per group) from saline (top panels)- and imiquimod (bottom panels)-administered WT mice exposed to normal air (left panels) or CS (right panels) for 8 weeks. Scale bars, 200 µm. (**j**) Quantification of small airway epithelial cell area per µm of basement

membrane (BM) perimeter (4 small airways per mouse, n = 6 mice per group) and representative micrographs (right panels) of small airways in H&E-stained lung sections from saline (top panels)- and imiquimod (bottom panels)-administered WT mice exposed to normal air (left panels) or CS (right panels) for 8 weeks. Scale bars, 50 μm. (**k**) Quantification of nuclei numbers per 100 μm of BM perimeter (4 small airways per mouse, n = 6 mice per group) and representative micrographs (right panels) showing small airway epithelial cell nuclei in H&E-stained lung sections from saline (top panels)- and imiquimod (bottom panels)-administered WT mice exposed to normal air (left panels) or CS (right panels) for 8 weeks. Scale bars, 20 μm. (**l**) *Ifna*, (**m**) *Ifnb*, (**n**) *Ifng*, (**o**) *Ifnl* and (**p**) *Ifnar1* mRNA levels in whole lung homogenates from saline- and imiquimod-administered WT mice exposed to normal air or CS for 8 weeks (n = 8 mice per group). mRNA data were normalized to the house-keeping *Hprt* transcript and expressed as relative abundance to saline-administered WT controls. All data are presented as means ± s.e.m. *P< 0.05; **P< 0.01; ***P< 0.001; ****P< 0.0001 compared to saline- or imiquimod-administered WT mice exposed to normal air, and $^{\#}P$< 0.05 compared to imiquimod-administered WT mice exposed to CS by one-way ANOVA with Bonferonni's multiple comparison test; ns, not significant.

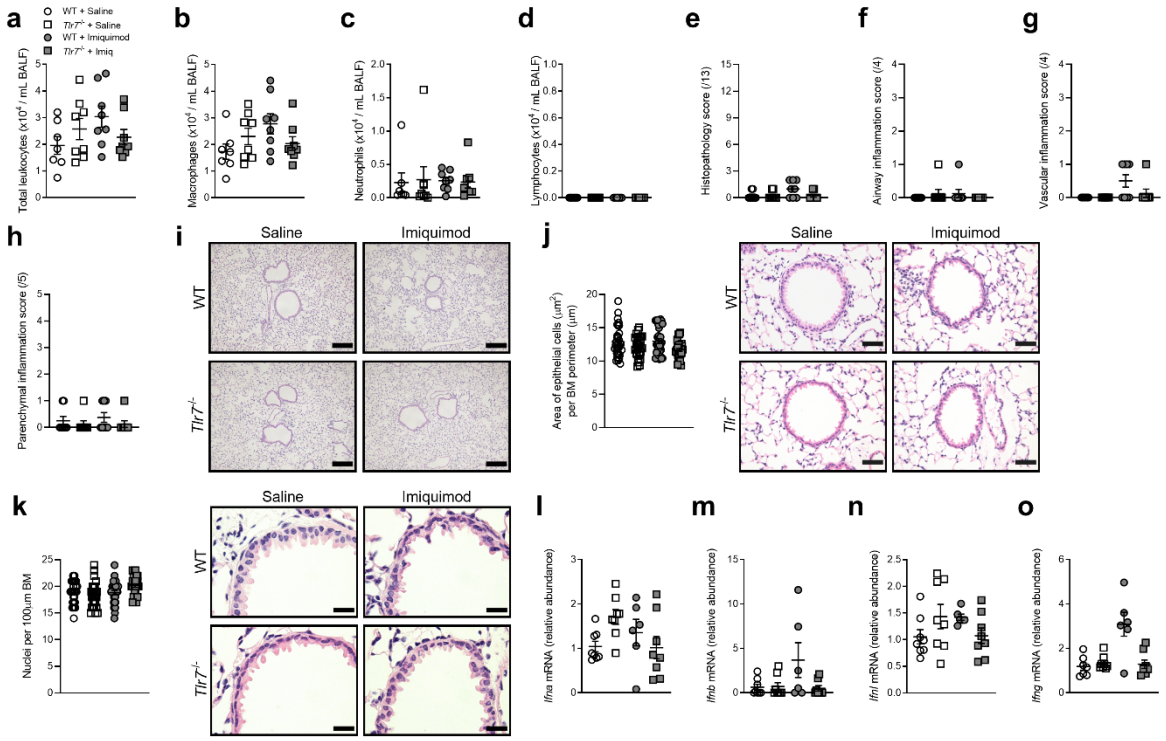

Supplementary Figure 5 | Administration of imiquimod does not affect pulmonary inflammation or small airway remodelling in *Tlr7*$^{-/-}$ mice. WT or *Tlr7*$^{-/-}$ mice were administered imiquimod (50 µg) in sterile saline, intranasally 5 times per week, for 2 weeks. Controls received sterile saline. (**a**) Total leukocytes, (**b**) macrophages, (**c**) neutrophils and (**d**) lymphocytes in May-Grunwald Giemsa stained BALF cytospins from WT and *Tlr7*$^{-/-}$ mice administered saline or imiquimod (n = 8 mice per group). (**e – h**) Histopathology scores and (**i**) representative micrographs of H&E-stained lung sections (n = 8 mice per group) from WT (top panels) and *Tlr7*$^{-/-}$ (bottom panels) mice administered saline (left panels) or imiquimod (right panels). Scale bars, 200 µm. (**j**) Quantification of small airway epithelial cell area per µm of basement membrane (BM) perimeter (4 small airways per mouse, n = 8 mice per group) and representative micrographs (right panels) of small airways in H&E-stained lung sections from WT (top) and *Tlr7*$^{-/-}$ (bottom panels) mice administered saline (left panels) or imiquimod (right panels). Scale bars, 50 µm. (**k**) Quantification of nuclei numbers per 100 µm of BM perimeter (4 small airways per mouse, n = 8 mice per group) and representative micrographs (right

1362 panels) showing small airway epithelial cell nuclei in H&E-stained lung sections from WT (top
1363 panels) and *Tlr7*$^{-/-}$ (bottom panels) mice administered saline (left panels) or imiquimod (right
1364 panels). Scale bars, 20 μm. (**l**) *Ifna*, (**m**) *Ifnb*, (**n**) *Ifng* and (**o**) *Ifnl* mRNA levels in whole lung
1365 homogenates from saline- and imiquimod-administered WT or *Tllr7*$^{-/-}$ mice exposed to normal
1366 air or CS for 8 weeks (n = 8 mice per group). mRNA data were normalized to the house-keeping
1367 *Hprt* transcript and expressed as relative abundance to saline-administered WT controls. All
1368 data are presented as means ± s.e.m.

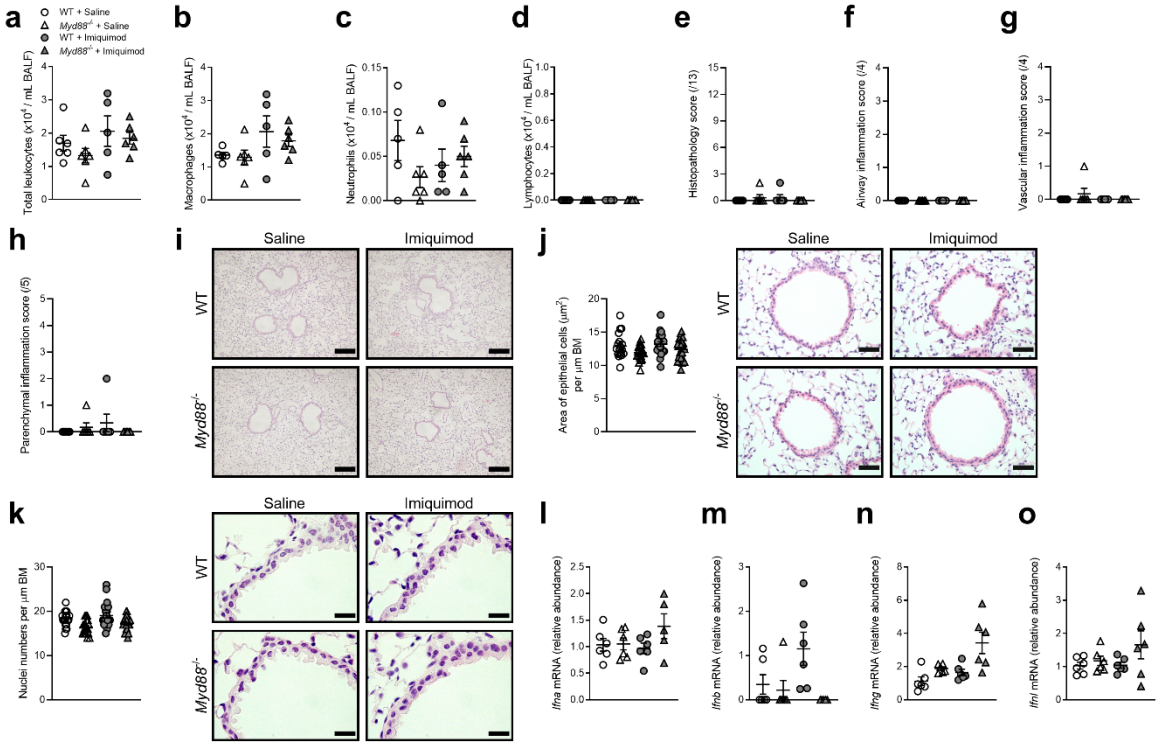

Supplementary Figure 6 | Administration of imiquimod does not affect pulmonary inflammation or small airway remodelling in *Myd88*$^{-/-}$ mice. WT or *Myd88*$^{-/-}$ mice were administered imiquimod (50 µg) in sterile saline, intranasally 5 times per week, for 2 weeks. Controls received sterile saline. (**a**) Total leukocytes, (**b**) macrophages, (**c**) neutrophils and (**d**) lymphocytes in May-Grunwald Giemsa stained BALF cytospins from WT and *Myd88*$^{-/-}$ mice administered saline or imiquimod (n = 6 mice per group). (**e – h**) Histopathology scores and (**i**) representative micrographs of H&E-stained lung sections (n = 6 mice per group) from WT (top panels) and *Myd88*$^{-/-}$ (bottom panels) mice administered saline (left panels) or imiquimod (right panels). Scale bars, 200 µm. (**j**) Quantification of small airway epithelial cell area per µm of BM perimeter (4 small airways per mouse, n = 6 mice per group) and representative micrographs (right panels) of small airways in H&E-stained lung sections from WT (top panels) and *Myd88*$^{-/-}$ (bottom panels) mice administered saline (left panels) or imiquimod (right panels). Scale bars, 50 µm. (**k**) Quantification of nuclei numbers per 100 µm of BM perimeter (4 small airways per mouse, n = 6 mice per group) and representative micrographs (right

1384 panels) showing small airway epithelial cell nuclei in H&E-stained lung sections from WT (top
1385 panels) and *Myd88*$^{-/-}$ (bottom panels) mice administered saline (left panels) or imiquimod (right
1386 panels). Scale bars, 20 μm. (**l**) *Ifna*, (**m**) *Ifnb*, (**n**) *Ifng* and (**o**) *Ifnl* mRNA levels in whole lung
1387 homogenates from saline- and imiquimod-administered WT or *Myd88*$^{-/-}$ mice (n = 6 mice per
1388 group). mRNA data were normalized to the house-keeping *Hprt* transcript and expressed as
1389 relative abundance to saline-administered WT controls. Throughout, data are presented as
1390 means ± s.e.m.

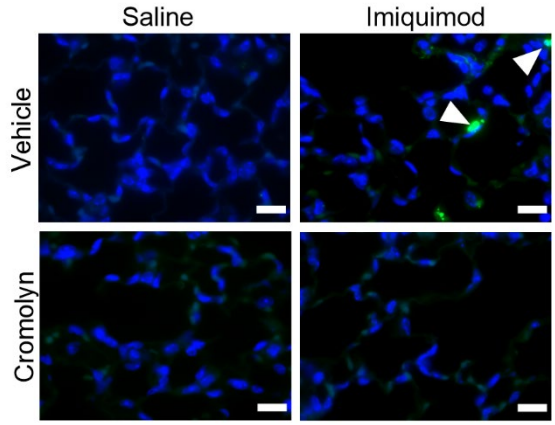

Supplementary Figure 7 | Mast cell stabilizer cromolyn reduces imiquimod-induced apoptosis. WT mice were first treated with vehicle (sterile water) or cromolyn (50 mg/kg body weight) 2 hours prior to administration of sterile saline or imiquimod (50 μg), intranasally 5 times per week, for 2 weeks. Representative micrographs of TUNEL-stained lung sections (*n* = 8 mice per group) from vehicle- (top panels) or cromolyn (bottom panels)-treated mice administered saline (left panels) or imiquimod (right panels). Arrows indicate $TUNEL^+$ cells. Scale bars, 20 μm.

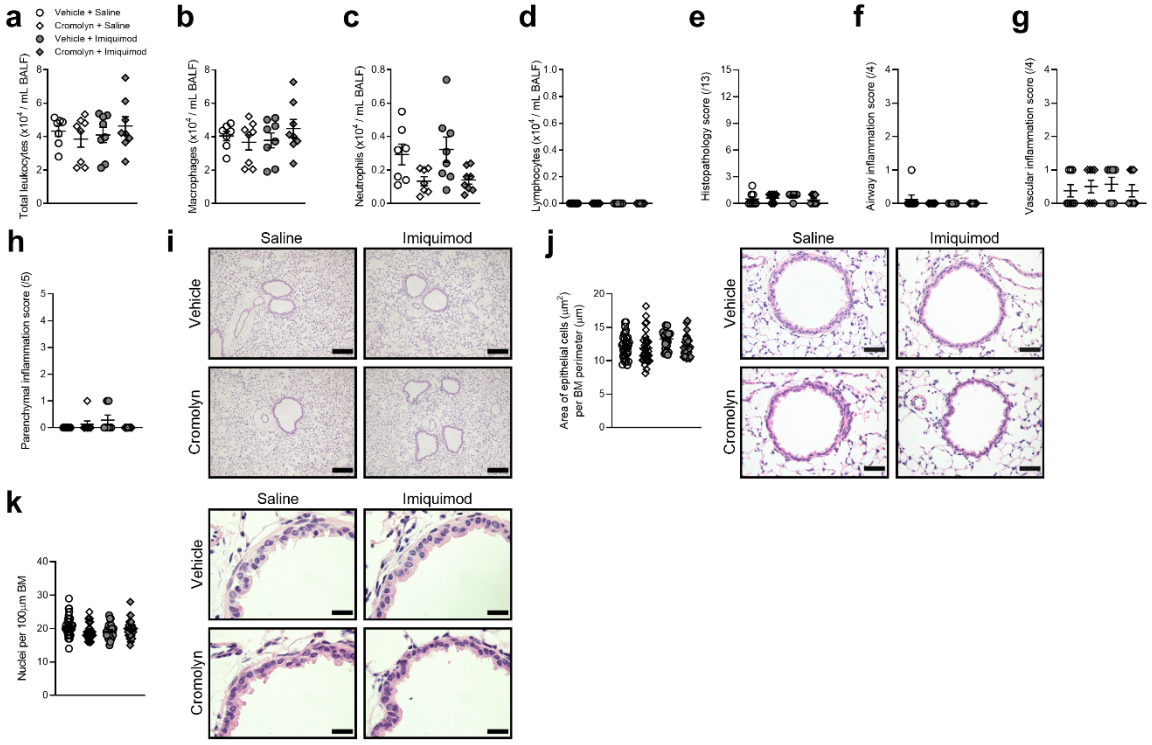

Supplementary Figure 8 | Administration of mast cell stabilizer cromolyn with or without imiquimod does not affect pulmonary inflammation or small airway remodelling. WT mice were first treated with vehicle (sterile water) or cromolyn (50 mg/kg body weight) 2 hours prior to administration of sterile saline or imiquimod (50 µg), intranasally 5 times per week, for 2 weeks. (**a**) Total leukocytes, (**b**) macrophages, (**c**) neutrophils and (**d**) lymphocytes in May-Grunwald Giemsa stained BALF cytospins from vehicle- or cromolyn-treated mice administered saline or imiquimod (n = 8 mice per group). (**e – h**) Histopathology scores and (**i**) representative micrographs of H&E-stained lung sections (n = 6 mice per group) from vehicle- (top panels) and cromolyn-treated (bottom panels) mice administered saline (left panels) or imiquimod (right panels). Scale bars, 200 µm. (**j**) Quantification of small airway epithelial cell area per µm of BM perimeter (4 small airways per mouse, n = 8 mice per group) and representative micrographs (right panels) of small airways in H&E-stained lung sections from vehicle- (top panels) and cromolyn-treated (bottom panels) mice administered saline (left panels) or imiquimod (right panels). Scale bars, 50 µm. (**k**) Quantification of nuclei numbers

per 100 μm of BM perimeter (4 small airways per mouse, n = 6 mice per group) and representative micrographs (right panels) showing small airway epithelial cell nuclei in H&E-stained lung sections from vehicle- (top panels) and cromolyn-treated (bottom panels) mice administered saline (left panels) or imiquimod (right panels). Scale bars, 20 μm. Throughout, data are presented as means ± s.e.m.

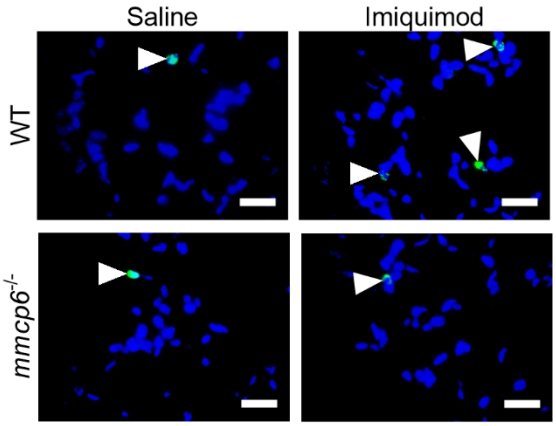

Supplementary Figure 9 | Imiquimod-induced apoptosis is reduced in *mmcp6*$^{-/-}$ mice. WT or *mmcp6*$^{-/-}$ mice were administered imiquimod (50 µg) in sterile saline, intranasally 5 times per week, for 2 weeks. Controls received sterile saline. Representative micrographs of TUNEL-stained lung sections (n = 6 mice per group) from WT (top panels) or *mmcp6*$^{-/-}$ (bottom panels) mice administered saline (left panels) or imiquimod (right panels). Arrows indicate TUNEL^{+} cells. Scale bars, 20 µm.

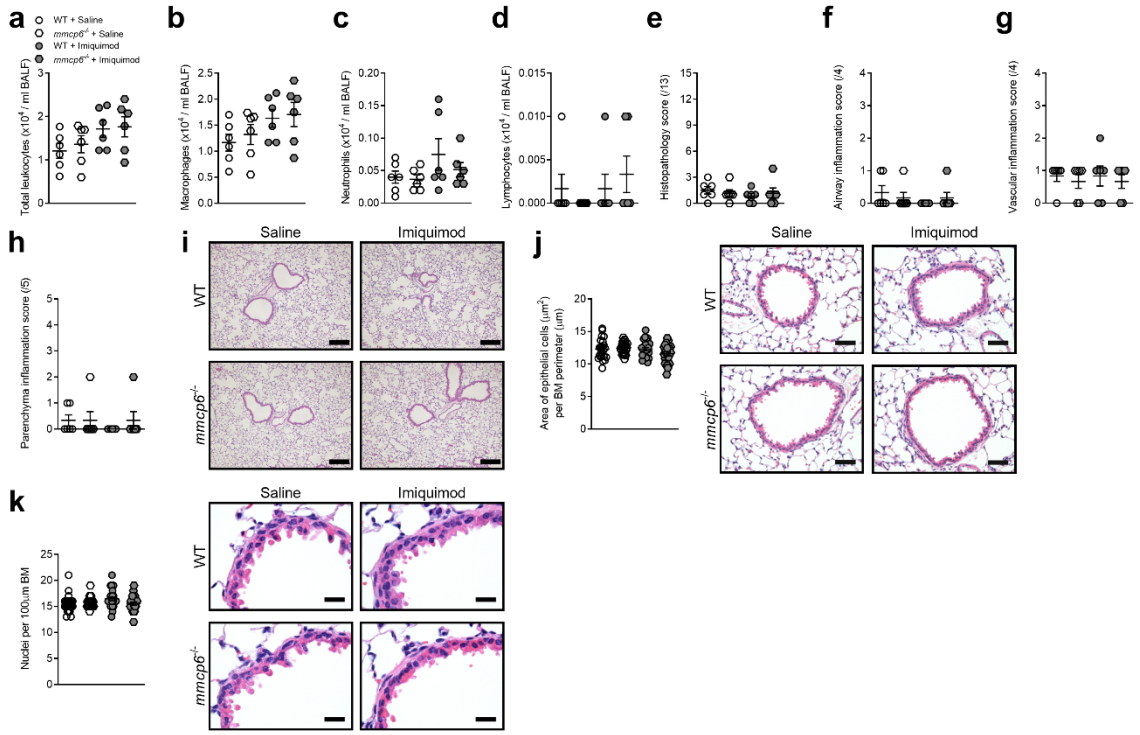

Supplementary Figure 10 | Administration of imiquimod does not affect pulmonary inflammation or small airway remodelling in *mMCP6*$^{-/-}$ mice. WT or *mMCP6*$^{-/-}$ mice were administered imiquimod (50 µg) in sterile saline, intranasally 5 times per week, for 2 weeks. Controls received sterile saline. (**a**) Total leukocytes, (**b**) macrophages, (**c**) neutrophils and (**d**) lymphocytes in May-Grunwald Giemsa stained BALF cytospins from WT and *mMCP6*$^{-/-}$ mice administered saline or imiquimod (n = 6 mice per group). (**e – h**) Histopathology scores and (**i**) representative micrographs of H&E-stained lung sections (n = 6 mice per group) from WT (top panels) and *mMCP6*$^{-/-}$ (bottom panels) mice administered saline (left panels) or imiquimod (right panels). Scale bars, 200 µm. (**j**) Quantification of small airway epithelial cell area per µm of BM perimeter (4 small airways per mouse, n = 6 mice per group) and representative micrographs (right panels) of small airways in H&E-stained lung sections from WT (top panels) and *mMCP6*$^{-/-}$ (bottom panels) mice administered saline (left panels) or imiquimod (right panels). Scale bars, 50 µm. (**k**) Quantification of nuclei numbers per 100 µm of BM perimeter (4 small airways per mouse, n = 6 mice per group) and representative micrographs

1441 (right panels) showing small airway epithelial cell nuclei in H&E-stained lung sections from
1442 WT (top panels) and *mMCP6*$^{-/-}$ (bottom panels) mice administered saline (left panels) or
1443 imiquimod (right panels). Scale bars, 20 μm. Throughout, data are presented as means ± s.e.m.

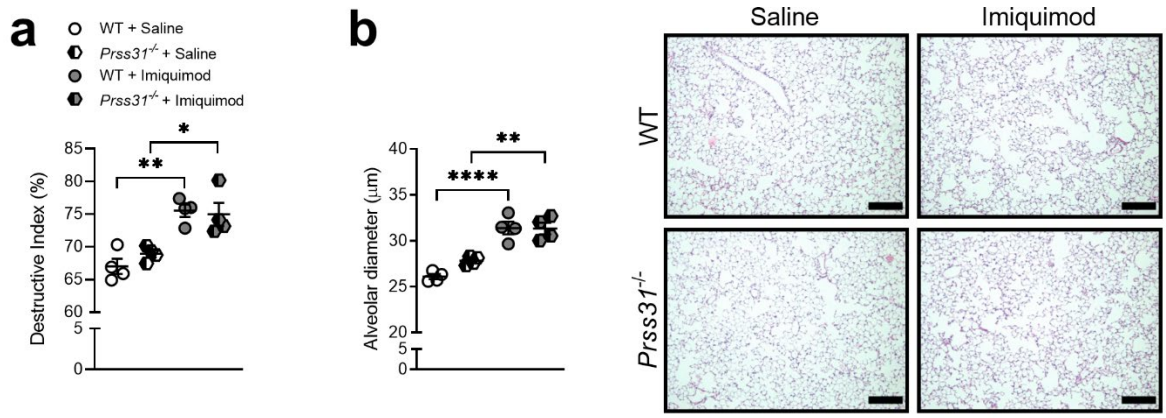

Supplementary Figure 11 | Imiquimod-induced emphysema is not altered in *Prss31*$^{-/-}$ mice. WT or *Prss31*$^{-/-}$ mice were administered imiquimod (50 μg) in sterile saline, intranasally 5 times per week, for 2 weeks. Controls received sterile saline. (**a**) Quantification of destructive index (n = 4 mice per group) of saline- or imiquimod-administered WT and *Prss31*$^{-/-}$ mice. (**b**) Quantification of mean linear intercept (n = 4 mice per group) and representative micrographs (right) of H&E-stained lung sections from WT (top panels) and *Prss31*$^{-/-}$ (bottom panels) mice administered saline (left panels) or imiquimod (right panels). Scale bars, 200 μm. Throughout, data are presented as means ± s.e.m. **P*< 0.05; ***P*< 0.01; *****P*< 0.0001 compared to saline-administered WT or *Prss31*$^{-/-}$ mice by one-way ANOVA with Bonferonni's multiple comparison test.

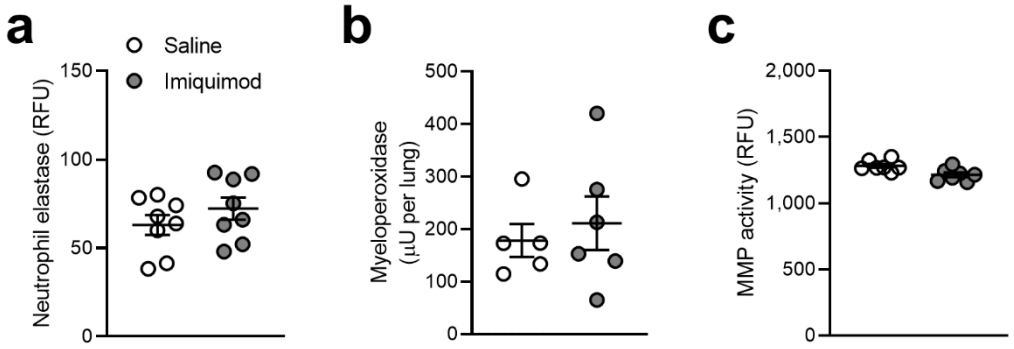

Supplementary Figure 12 | Administration of imiquimod does not affect other known proteases in the lung. WT mice were administered imiquimod (50 μg) in sterile saline, intranasally 5 times per week for 8 weeks. Controls received sterile saline. Quantification of (**a**) neutrophil elastase, (**b**) myeloperoxidase and (**c**) total matrix metalloproteinase (MMP) activities in the lungs of WT mice administered saline or imiquimod (n = 6 mice per group). Throughout, data are presented as means ± s.e.m.

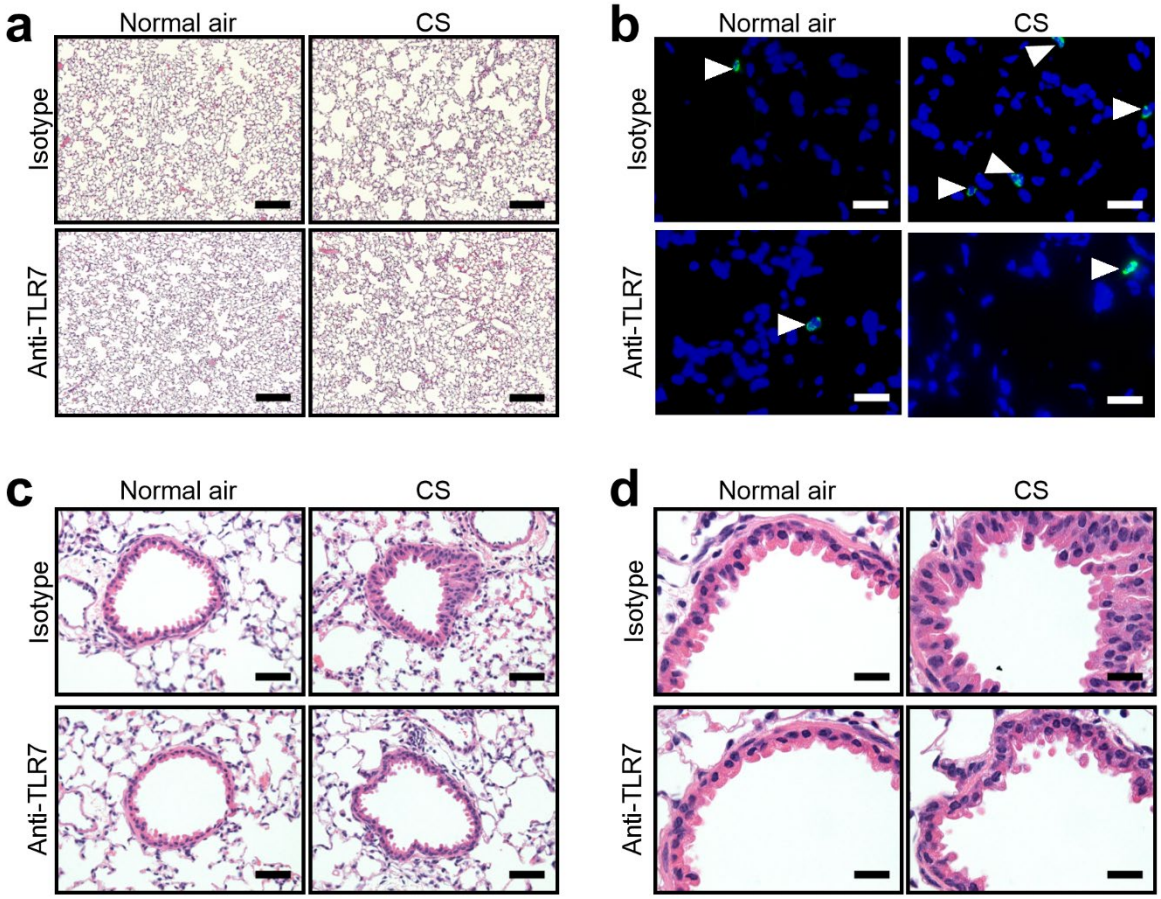

Supplementary Figure 13 | Neutralization of TLR7 reduces emphysema and small airway remodelling in experimental COPD. WT mice were exposed to normal air or CS for 8 weeks and administered neutralizing anti-TLR7 monoclonal antibody or isotype control, intravenously (i.v.) once per week, between Week 6 to 8 (for 2 weeks). (**a**) Representative micrographs (n = 6 mice per group) of H&E-stained lung sections from isotype (top panels)- or anti-TLR7 (bottom panels)-treated WT mice exposed to normal air (left panels) or CS (right panels) for 8 weeks. Scale bars, 200 µm. (**b**) Representative micrographs (n = 6 mice per group) of TUNEL-stained lung sections from isotype (top panels)- or anti-TLR7 (bottom panels)-treated WT mice exposed to normal air (left panels) or CS (right panels) for 8 weeks. Arrows indicate $TUNEL^+$ cells. Scale bars, 20 µm. Representative micrographs (n = 6 mice per group) of (**c**) small airways and (**d**) small airway epithelial cell nuclei in H&E-stained lung sections

from isotype (top panels)- or anti-TLR7 (bottom panels)-treated WT mice exposed to normal air (left panels) or CS (right panels) for 8 weeks. Scale bars, 20 μm.

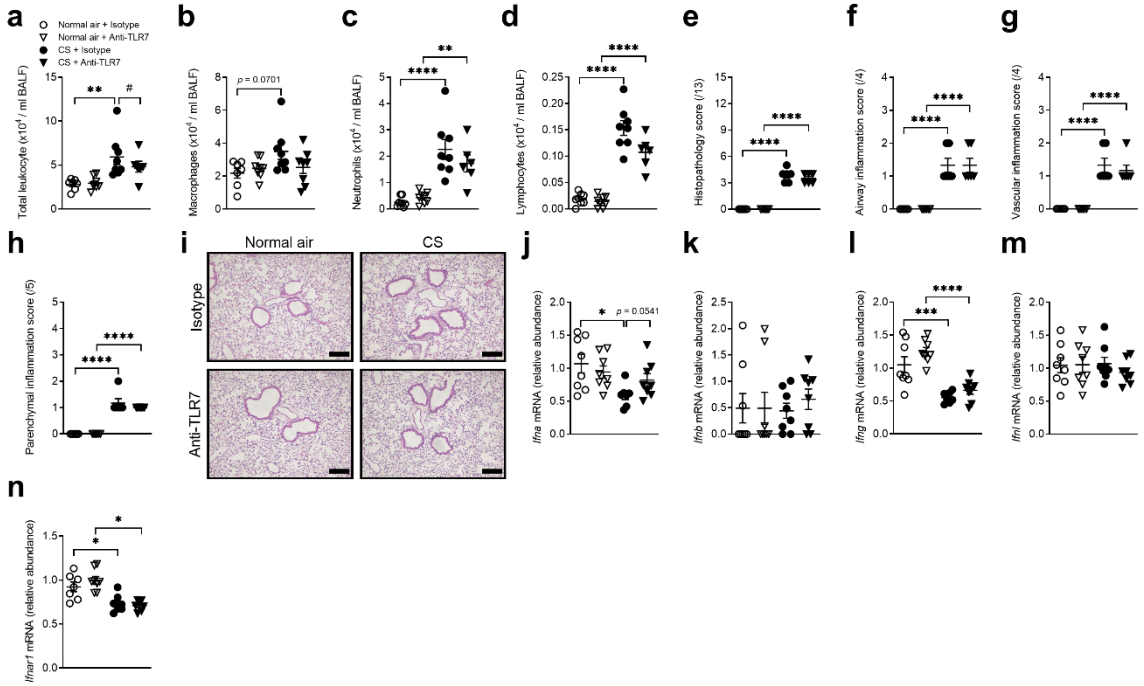

Supplementary Figure 14 | Neutralization of TLR7 has modest effects on pulmonary inflammation and small airway remodelling in experimental COPD. WT mice were exposed to normal air or CS for 8 weeks and administered neutralizing anti-TLR7 monoclonal antibody or isotype control, intravenously (i.v.) once per week, between Week 6 to 8 (for 2 weeks). (**a**) Total leukocytes, (**b**) macrophages, (**c**) neutrophils and (**d**) lymphocytes in May-Grunwald Giemsa stained BALF cytospins from isotype- and anti-TLR7-treated WT mice exposed to normal air or CS for 8 weeks (n = 8 mice per group). (**e – h**) Histopathology scores and (**i**) representative micrographs of H&E-stained lung sections (n = 8 mice per group) from isotype (top panels)- and anti-TLR7 (bottom panels)-treated WT mice exposed to normal air (left panels) or CS (right panels). Scale bars, 200 µm. (**j**) *Ifna*, (**k**) *Ifnb*, (**l**) *Ifng* (**m**) *Ifnl* and (**n**) *Ifnar1* mRNA levels in whole lung homogenates by qPCR from isotype- and anti-TLR7-treated WT mice exposed to normal air or CS for 8 weeks (n = 8 mice per group). mRNA data were normalized to house-keeping *Hprt* transcript and expressed as relative abundance to saline-administered WT controls. Throughout, data are presented as means ± s.e.m. *P< 0.05; **P< 0.01; ***P< 0.001; ****P< 0.0001 compared to isotype- or anti-TLR7-administered WT mice

exposed to normal air, and $^{\#\#\#\#}P<$ 0.0001 compared to anti-TLR7-administered WT mice exposed to CS by one-way ANOVA with Bonferonni's multiple comparison test.

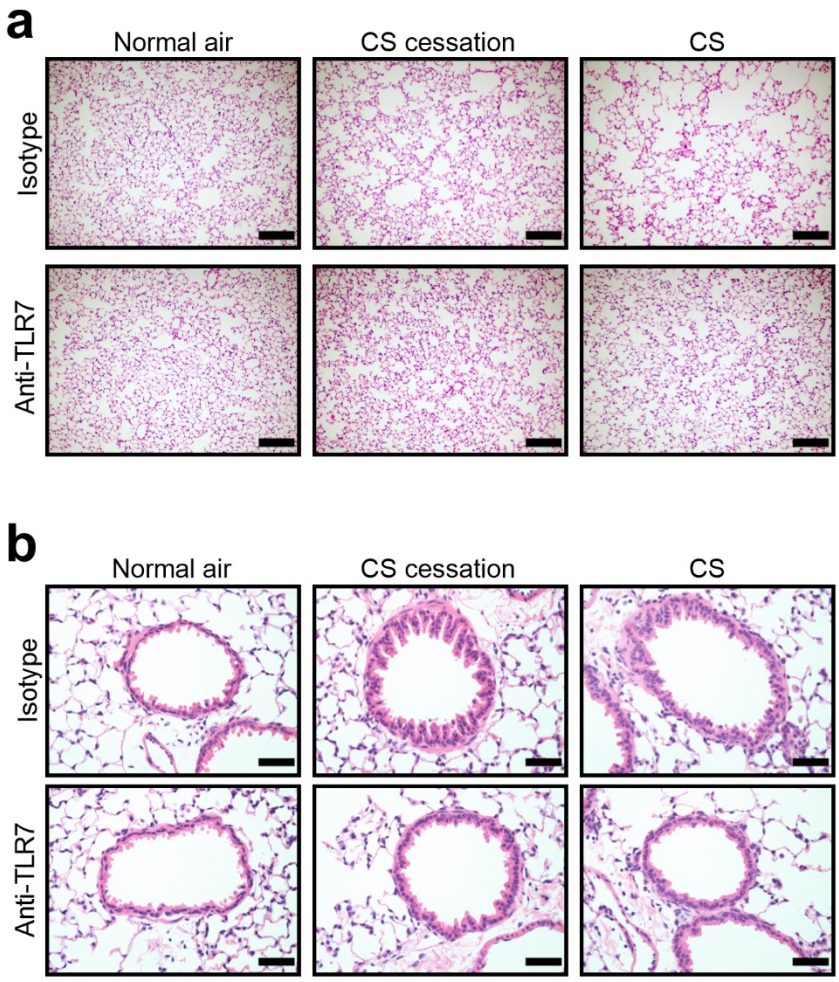

Supplementary Figure 15 | Neutralization of TLR7 during disease progression in a 12-week experimental COPD model reduces emphysema and small airway remodelling. WT mice were exposed to normal air or CS for 12 weeks and some groups underwent CS cessation after 8 week of CS exposure. Mice were treated with either neutralizing anti-TLR7 monoclonal antibody or isotype control, intravenously once per week, between Week 8 to 12 (for 4 weeks). (**a**) Representative micrographs (n = 5-6 mice per group) of H&E-stained lung sections from isotype (top panels)- and anti-TLR7 (bottom panels)-treated WT mice exposed to normal air (left panels) or CS (right panels) for 12 weeks and those with CS cessation (middle panels). Scale bars, 200 µm. (**b**) Representative micrographs (4 small airways per mouse, n = 5-6 mice per group) of small airways in H&E-stained lung sections from isotype (top panels)- and anti-

TLR7 (bottom panels)-treated WT mice exposed to normal air (left panels) or CS (right panels) for 12 weeks and those with CS cessation (middle panels). Scale bars, 50 μm.

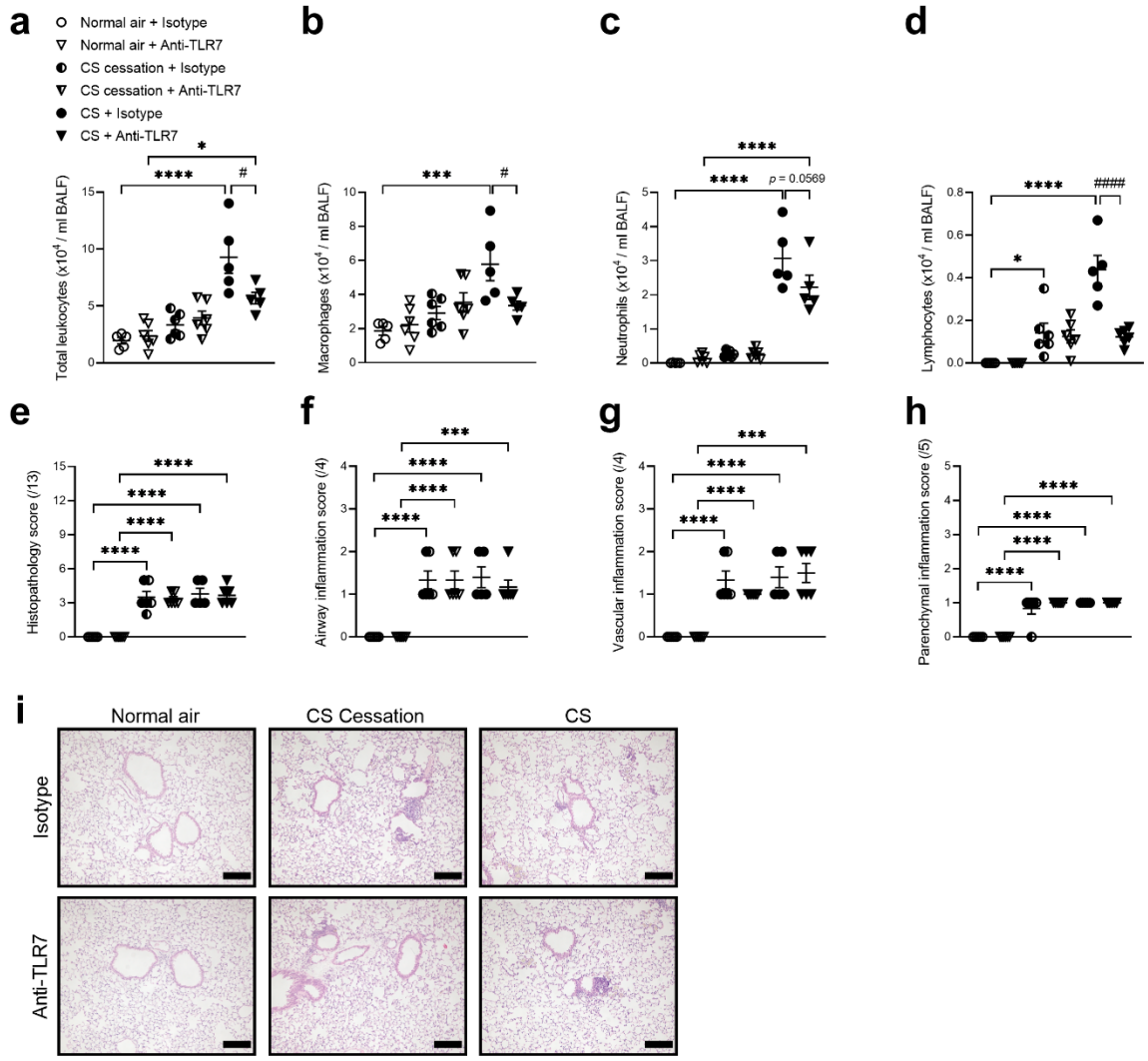

Supplementary Figure 16 | Neutralization of TLR7 during disease progression in a 12-week experimental COPD model reduced inflammation. WT mice were exposed to normal air or CS for 12 weeks and some groups underwent CS cessation after 8 week of CS exposure. Mice were treated with either neutralizing anti-TLR7 monoclonal antibody or isotype control, intravenously once per week, between Week 8 to 12 (for 4 weeks). (**a**) Total leukocytes, (**b**) macrophages, (**c**) neutrophils and (**d**) lymphocytes in May-Grunwald Giemsa stained BALF cytospins from isotype- and anti-TLR7-administered WT mice exposed to normal air or CS for 12 weeks and with or with CS cessation (n = 6 mice per group). (**e – h**) Histopathology scores and (**i**) representative micrographs of H&E-stained lung sections (n = 6 mice per group) from isotype (top panels)- and anti-TLR7 (bottom panels)-administered WT mice exposed to normal

air (left panels) or CS (right panels) and with or with CS cessation (middle panels). Throughout, data are presented as means ± s.e.m. *P< 0.05; **P< 0.01; ***P< 0.001; ****P< 0.0001 compared to isotype- or anti-TLR7-treated WT mice exposed to normal air, and $^{\#}P$< 0.05; $^{\#\#\#\#}P$< 0.0001 compared to anti-TLR7-treated WT mice exposed to CS for 12 weeks or those with CS cessation by one-way ANOVA with Bonferonni's multiple comparison test.